Performance assessment of a predictive pre-heating strategy for a hybrid electric vehicle equipped with an electrically heated catalyst

Published Version:
Canè S., Brunelli L., Gallian S., Perazzo A., Brusa A., Cavina N. (2023). Performance assessment of a predictive pre-heating strategy for a hybrid electric vehicle equipped with an electrically heated catalyst. APPLIED THERMAL ENGINEERING, 219(A), 1-20 [10.1016/j.applthermaleng.2022.119341].

Availability:
This version is available at: https://hdl.handle.net/11585/898988 since: 2024-05-10

Published:
DOI: http://doi.org/10.1016/j.applthermaleng.2022.119341

Performance assessment of a predictive pre-heating strategy for a hybrid electric vehicle equipped with an electrically heated catalyst

Stella Canè, Lorenzo Brunelli, Sara Gallian, Alessandro Perazzo, Alessandro Brusa, Nicolò Cavina

Abstract

In recent years, hybrid electric vehicles have been recognized as a valid solution in response to increasingly tight regulations on CO_2 emission. However, reduced engine load and repeated engine starts and stops may reduce substantially the temperature of the exhaust after-treatment system (EATS), leading to relevant issues related to pollutant emission control. In this context, electrically heated catalysts (EHCs) represent a promising solution to ensure high pollutant conversion efficiency without affecting engine efficiency and performance. This work aims at studying the advantages provided by the introduction of a predictive EHC control function for a light-duty Diesel plug-in hybrid electric vehicle (PHEV) equipped with a Euro 7-oriented EATS. Based on the knowledge of future driving scenarios provided by vehicular connectivity, engine first start can be predicted and therefore an EATS pre-heating phase can be planned. For this purpose, a representative 0-D model has been considered to define the most convenient pre-heating strategy and different real driving scenarios have been simulated to test the proposed EHC predictive control strategy. Although the pre-heating introduction implies an additional energy request which results in increased fuel consumption, the results show that the final NO_x emission over a complete driving cycle can be reduced up to more than 60% compared to the base EHC strategy. Moreover, this would allow to comply with the scenarios introduced by the Euro 7 regulation proposal, while enabling the adoption of a simplified EATS architecture resulting in reduced manufacturing costs.

1 Introduction

In the last decades, European regulations on CO_2 and pollutant emissions have become increasingly strict for almost the entire vehicle fleet, covering transport classes that go from passenger cars to heavy-duty applications [1], [2]. In this context, vehicle hybridization has proven to be an effective and feasible solution to improve engine efficiency and significantly reduce CO_2 emissions, as evidenced by [3], in which real-world CO_2 emissions of different hybrid electric vehicles (HEVs) are evaluated and critically analyzed. The potential of vehicle hybridization further increases when coupled with advanced combustion systems, like RCCI engines, bringing benefits both in terms of fuel consumption and engine-out emissions [4]. In parallel, the coupling with advanced exhaust after-treatment systems (EATS), allows to limit tailpipe pollutant emissions at the same time to comply with the targets imposed by the regulations, thanks to the latest progress in the field of pollutant conversion technologies for both Diesel and gasoline applications [5], [6]. Nonetheless, significant issues can still be experienced due to cold operation of the after-treatment devices during engine start and warm-up, resulting in low pollutant conversion efficiency, as widely evidenced by [7]. In fact, experimental tests and measurements as the ones in [8] and [9], clearly pointed out that frequent engine on/off transitions and low load operation, which commonly characterize HEVs operation with respect to standard vehicles, may have a strong, negative impact on EATS operation and performance due to a substantial reduction of EATS temperature [8], [7]. The same issue is pointed out also by [10], which shows a comparison in terms of pollutant emissions between a conventional and a hybridized vehicle during cold starts, then highlighting the potential of an optimized energy management strategy which considers also catalyst efficiency as an additional constraint to significantly reduce tailpipe emissions. Moreover, as highlighted by [7], another critical situation that may occur in HEVs is the so-called internal combustion engine (ICE) high-power cold start, when the engine is forced to start to support the electric machine (EM) in case of a sudden transition from low to high torque request. In this situation, the engine must go from an off-state to a high-load state as fast as possible to fulfill the driver demand, and if it happens after an extended e-drive phase, the EATS temperature can be very low, thus strongly affecting the resulting pollutant emissions, as supported by the experimental results presented in [11].

Therefore, many technologies and strategies have been developed trying to solve this problem, including methods based on engine calibration, torque split management, and EATS layout, as widely reviewed in [12]. However, thermal management methods based on engine calibration, including late combustion, post-injection, idle speed increase, variable valve timing, and wastegate valve control show a limited potential due to their significant fuel penalty and performance degradation during cold start. Nonetheless, they do not require the installation of any additional device, which is a significant advantage. A further solution that can be applied to hybrid vehicles is acting on the additional degree of freedom given by the torque split management to improve catalyst conversion efficiency. In particular, in [13] an energy management strategy that takes into account catalyst temperature as a soft constraint is developed, enabling the rapid warm-up of the catalyst and significantly reducing tailpipe HC, CO, and NO_x, even if a slight increase of fuel consumption is observed. These results are confirmed also by [14], which investigates the optimal torque distribution to reach a trade-off between limited pollutant emissions and high hybrid powertrain efficiency. However, even if optimized hybrid strategies can bring a significant improvement in terms of pollutant emissions with limited fuel consumption penalties, they could not solve the issue related to the very first engine start and especially to high-power cold starts. On the other hand, acting on the EATS layout, the installation of after-burners or reformers, coupled with secondary air introduction in the first case, allows to strongly speed-up catalyst heating phase. But, even if these methods are very effective and do not affect engine operation, they imply important fuel penalties and significant additional costs. An additional solution to improve EATS thermal management is to integrate a thermal energy storage (TES) system into the catalytic converter to absorb the exhaust gas thermal energy as latent heat during engine high-load operation and gradually release it back to the catalyst substrate when the engine is off. This method has the advantage of not causing additional energy consumption and, as shown in [15], it has great potential in improving the emissions reduction performance particularly for hybrid vehicles, by avoiding the catalyst to light-out after the cold-start. However, the effectiveness of these systems strongly depends on the time interval between an engine-off and the next engine start and in the worst case the catalyst light-off time could be even prolonged if the heat storage material is cold after a long engine stop.

In this context, according to the state of the art, electrically heated catalysts (EHCs), employing one or more discs upstream of the catalyst that are heated by an electric resistance, provide an effective solution to reduce emissions during engine cold start without affecting engine performance and without the limits evidenced for TES systems [16].

1.1 Related works and novel contribution

In [17] a novel EHC control strategy is investigated to increase DOC conversion efficiency minimizing EHC electric energy consumption; the results show that a reduction of more than 70% of the cumulative CO and HC emission can be reached with respect to a standard post-injection strategy. According to [18], the implementation of a 12V electrical heater to a standard Diesel EURO 6 EATS leads to a significant reduction of the overall pollutant emission, reaching more than 60% of cumulative NO_x emission reduction along a cold start WLTC. The CO_2 percentage penalty due the additional EHC energy consumption in also evaluated, showing values in the range of 6 ÷9% depending on the considered EHC control strategy. In [19] the performance in terms of CO_2 and NO_x emission of a 48V P0 Diesel hybrid equipped with an EHC are compared to those from a conventional non-hybrid vehicle. The results show that, despite the fuel consumption penalty, thanks to the EHC the NO_x level can be reduced significantly especially during city and short-distance drives, while for the same NO_x emissions level a CO_2 saving of 7 % can be achieved. The effect of the addition of an EHC on the behavior of a DOC in a hybrid RCCI truck is studied in [20]; in particular, it shows that the electrical heating helps reducing HC and CO emissions, which is the main challenge related to high-efficiency low-temperature combustion systems, even if in some cases the EURO 6 limits are exceeded anyway. In [21] the effectiveness of pre-heating a PHEV's after-treatment system by means of a 48V EHC is evaluated. A reduction of more than 50% of the cumulative NO_x emission related to the first engine start is observed along the considered test cycle, showing the potential of such a system in solving the issue related ICE high-power cold start. In [22] CFD simulation is used to study the effect of pre-heating through an EHC on emission characteristics of a motorcycle engine in cold-start conditions, evaluating the best position of the heating disc with respect to the catalyst and optimizing the pre-heating duration. According to the results, the highest CO reduction is observed with the electrical heater positioned upstream of the catalyst and when the heating is activated 35 s before engine start. In [23] an innovative conductive ceramic composite material is considered for the SCR catalyst support for a Diesel passenger vehicle; the investigated material allows direct electrical heating of the catalytic converter, thus reducing the light-off time up to one third with respect to the base system if a pre-heating phase is considered. As in [21] and [22], the potential of the introduction of an EATS pre-heating phase for reducing tailpipe pollutant emissions is highlighted, introducing also the issue of how to predict engine start.

Therefore, even if this heating method needs the installation of an additional device and the availability of a significant amount of electric energy to power it, the promising results reached in terms of reduced catalyst light-off time and improved catalyst conversion efficiencies justify further development of this technology, especially considering the current powertrain electrification trend, which makes available the electrical power needed by the EHC.

In addition, focusing on the highest degrees of hybridization, which means full hybrid and plug-in hybrid vehicles, the advantages and flexibility introduced by this technology are even clearer if integrated with a predictive control strategy. In fact, improvements in the vehicle-to-everything (V2X) communication technology, including vehicle-to-vehicle (V2V), vehicle-to-infrastructure (V2I), and vehicle-to-network (V2N) communication, together with the latest Advanced Driver-Assistance Systems (ADAS), allow calculating an electronic horizon (eHorizon) which represents a virtual reconstruction of the trip ahead for a planned route. Such information can be used to manage the available energy more efficiently and sustainably, as it allows the development of predictive control strategies aimed to the combined optimization of energy consumption [24], [25], battery thermal management [26], and emissions control [27], [28], as widely highlighted by the literature. The same information about future driving conditions could be also employed for the management of specific EATS devices, for example by developing smart strategies to optimize particulate filter regeneration [29] or urea consumption of SCR systems [30].

Based on all these considerations, the idea behind this paper is to exploit the advantages deriving from a high-efficiency hybrid powertrain coupled with an advanced EATS, together with the availability of vehicular connectivity to solve the issues related to pollutant emissions. As previously mentioned, only few studies dealing with EHC applications to reduce pollutant emissions on HEVs have been carried out, especially if compared to other already introduced methods. Therefore, according to the authors, the potential of catalyst pre-heating by means of an electrical heater in reducing the overall emissions should be further investigated as one of the most effective and feasible solutions to solve the problem of cold starts on hybrid vehicles. The key enabler for the application of an EATS pre-heating to real driving cycles is the possibility to predict the engine start: therefore, this study proposes to take advantage from the knowledge of future vehicle operating conditions to predict engine first start and plan a pre-heating based on that to prevent cold start emissions. To the knowledge of the authors, the contribution of a similar EHC predictive control function based on navigation data has not been investigated yet.

1.2 Prospects for EURO 7 regulation

The introduction of improved EATS thermal management strategies would be a key factor to be compliant with the new Euro 7 regulation, which should come into force between 2025 and 2027, setting even more challenging targets in terms of pollutant emissions. More in detail, according to [31], the current draft of the regulation would require that the emission limits, besides being much lower than Euro 6 ones, are enforced in nearly any possible operating condition. Vehicle laboratory testing would be maintained only for CO_2 and pollutants that cannot be measured with PEMS (Portable Emission Measurement Systems), while a wider range of ambient temperatures and altitudes would be investigated during the road tests. Moreover, there would be no substantial limitations on the driving cycles to be considered for the vehicle homologating procedure: any driving cycle longer than 5 km and any possible performed maneuver will be considered valid for the homologation, since no more speed, acceleration and road grade limitations are provided. Focusing on pollutant emissions limits, two different scenarios have been proposed within the EURO 7 current draft, referred to as Scenario A and the more demanding Scenario B. The most significant updates with respect to EURO 6d in-force regulation introduced by the EURO 7 are summarized in

Table *1*. In particular, a very strong reduction of the allowed NO_x emissions is observed, which reaches almost the 90% for the most demanding scenario. NO_x emissions control will become critical considering this challenging limit and the new testing conditions which will increase the impact of cold start phases on the whole driving cycle. Therefore, car manufacturers would be required to adopt extremely advanced after-treatment technologies to fulfill such demanding emission standards, leading to increased and nearly unaffordable manufacturing costs [32]. In this context, an advanced EATS thermal management, that takes advantage of the available vehicle connectivity, would allow to better exploit the available EATS devices, improving their conversion efficiency in any operating condition, thus ensuring the

Table 1 – Comparison of testing methods and pollutant emissions limits on RDE cycles according to EURO6d in-force regulation and the EURO 7 proposal.

Parameter	EURO 6d	EURO 7 Scenario A	EURO 7 Scenario B
RDE Testing Methods			
Ambient temperature	Moderate: 0 ÷ 30°C Extended: -7 ÷ 35°C	-10 ÷ 40°C	
Average Speed	Urban: 15-40 km/h	-	
Altitude	Moderate: 0 –700m | Extended: 700 –1300m	-	
$v \bullet a_{pos}$ [95th]*	Limits defined in [33]	-	
Positive elevation	Total: <1200 [m/100km] Urban: <1200 [m/100km]	-	
Trip distance	Urban/Rural/Motorway >16 km each	> 5 km	
Emissions limits for Diesel engines			
NO_x [mg/km]	80	30	10
PN_{10} [#/km]	$6x10^{11}$	$1x10^{11}$	$6x10^{10}$
CO [mg/km]	500	300	100
CH_4 [mg/km]	-	10	5
N_2O [mg/km]	-	10	5

*The product between vehicle speed and acceleration is used to verify the compliance of trip dynamics.

compliance with the regulations, simplifying the EATS architecture, and minimizing the corresponding manufacturing cost.

The focus of this work is to evaluate the potential advantages provided by the introduction of an EHC predictive control function for a Diesel plug-in hybrid light commercial vehicle (LCV) equipped with a Euro 7-oriented EATS. In this regard, a 0-D validated numerical model is used to determine the effect of EHC heating power and secondary air flow rate on the light-off time of the considered EATS devices and therefore to define the most suitable heating strategy able to minimize tailpipe NO_x emission with limited additional energy consumption. Then, based on ICE first start prediction, an EATS pre-heating phase is planned, allowing to solve the main issue related to cold start NO_x emissions: this would allow to meet the likely limits introduced by the most demanding Euro 7 scenario and, in parallel, to consider the adoption of a simplified EATS layout, thus reducing the resulting manufacturing cost. The proposed strategy is applied to different real driving scenarios, and the results provided by the simulations are compared to the ones provided by the base control strategy and critically analyzed.

2 Materials and Methods

This section is divided into three parts: (i) vehicle model, (ii) control strategy, and (iii) case of study. Firstly, an overview of the modeling approach is given, with a particular focus on EATS thermal model. In the second part, the development and implementation of the proposed EHC predictive control strategy is fully described. The approach that has been adopted to define the best pre-heating strategy is also introduced. Lastly, a summary of the considered test cases and conditions to evaluate the contribution of the proposed control strategy to the resulting NO_x emissions reduction is presented.

2.1 Vehicle model

A comprehensive 0-D control-oriented vehicle model has been developed in MATLAB®/Simulink® for this application. As already mentioned, the modeled vehicle is a Diesel P2 PHEV classified as an LCV. The considered hybrid architecture, represented in Figure 1, provides high flexibility in terms of possible operating modes and torque split strategies. The location of the electric machine (EM), thanks to the separation clutch, allows to perform effective regenerative braking as well as pure electric drive. The combination of a 9.4 kWh high-voltage (HV) battery and a 90 kW/440 Nm electric motor ensures a significant all-electric range with a top speed that can reach 140 km/h. The electric power unit is paired with a 2.3-liter compression ignition engine and a 6-speed dual-clutch transmission. All the main vehicle specifications are listed in Table 2.

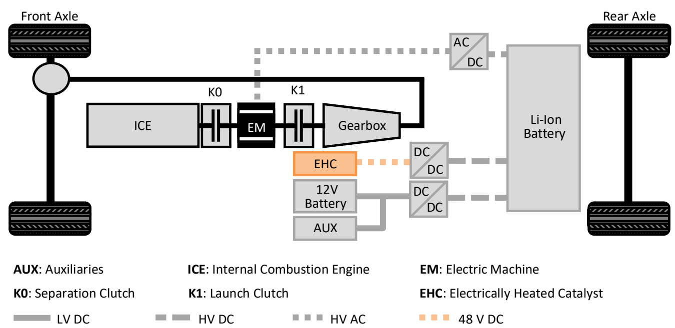

Figure 1 - Schematic representation of vehicle hybrid powertrain architecture.

Table 2 - Main powertrain and vehicle specifications.

Vehicle	Curb weight	2750 kg
	Configuration	P2, front wheel drive
Engine	Type	Diesel, turbocharged
	Displacement	2.3 l
	Rated power	95 kW @ 3000 rpm
	Rated torque	380 Nm @ 2000 rpm
	Gearbox	6-DCT
Electric machine	Type	PM synchronous
	Peak power	90 kW
	Peak/continuous torque	440/260 Nm
	Maximum speed	6000 rpm
Battery	Type	Lithium-ion polymer
	Capacity	9.4 kWh / 25.5 Ah
	Nominal voltage	370 V

2.1.1 Vehicle dynamics and powertrain model

An accurate analytical model has been adopted for both vehicle longitudinal dynamics and the electric power unit, including the EM and the HV battery. A detailed description and validation of the mentioned models are proposed in [34]. A map-based approach has been adopted for ICE modeling: fuel flow, exhaust gas temperature, and pollutant emissions maps allow calculating fuel consumption, turbine inlet temperature, and engine-out emissions of HC, CO, soot, and NO_x as a function of engine coolant temperature, load, and speed. All the data included in the mentioned maps have been obtained from previous activities and confidentially shared by FEV Italy. For completeness, fuel consumption and engine-out NO_x emission maps (Figure A 1, Figure A 2) have been included in the Appendix.

2.1.2 Exhaust after-treatment system model

As introduced in section 1, an advanced EATS is mandatory to meet the demanding targets imposed by the regulation in terms of pollutant emissions without affecting engine efficiency, while being compliant with CO_2 emissions limits. Therefore, the modeled vehicle is equipped with a Euro 7-oriented Diesel EATS, represented in Figure 2, which includes the following devices, with the corresponding volume V:

- Electrical heater;
- Diesel Oxidizing Catalyst (DOC), V=1.6 l;
- Low Thermal Mass Selective Catalytic Reduction (LTM-SCR) catalyst, V=1.2 l;
- SCR-coated Diesel Particulate Filter (SDPF), V=4.0 l;
- SCR catalyst, V=3.5 l.

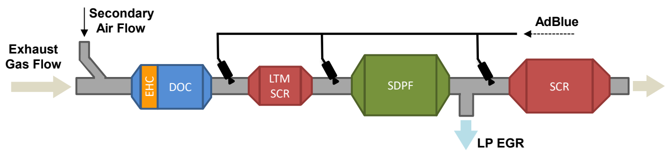

Figure 2 - Schematic representation of vehicle EATS architecture.

As pointed out by Figure 2, a secondary air flow is also provided: a gas flow through the heating disc is mandatory to transfer the heating power to the following devices along the exhaust line. This means that if a pre-heating phase is planned before the engine start, the air flow through the exhaust line must be provided by installing a secondary air pump upstream of the EHC. The pump is modeled by providing an additional air mass flow during pre-heating phases when the engine is not running. Then, the resulting power consumption is calculated depending on the supply voltage and air flow rate, according to the experimental data shown in Figure 3, derived from secondary air pumps available on the market.

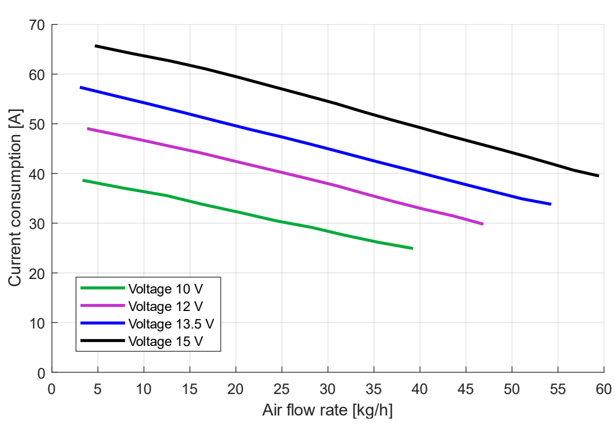

Figure 3 - Secondary air pumps: absorbed current for different supply voltages.

DOC conversion efficiency maps of HC, CO, and NO as a function of volumetric flow rate and gas average temperature allow to calculate the resulting pollutant emissions after the oxidizing reactions that take place in the DOC. Similarly, NO_x reduction performed by LTM-SCR, SDPF, and SCR is modeled for each device with a map based-approach, by firstly calculating NO_x conversion efficiency, which depends on gas average temperature, NO_2/NO_x ratio, and space velocity; all the mentioned maps of pollutants conversion efficiency for the different EATS devices have been obtained from experimental campaigns previously carried out within FEV and the related data are confidential. Then, from the knowledge of the conversion efficiency, it is possible to obtain the amount of NH_3 that can react to reduce NO_x, and thus the amount of AdBlue to be injected. Therefore, a comprehensive and robust EATS thermal model, which allows to correctly estimate the average temperature of each after-treatment device, is mandatory to obtain realistic results in terms of tailpipe pollutant emissions.

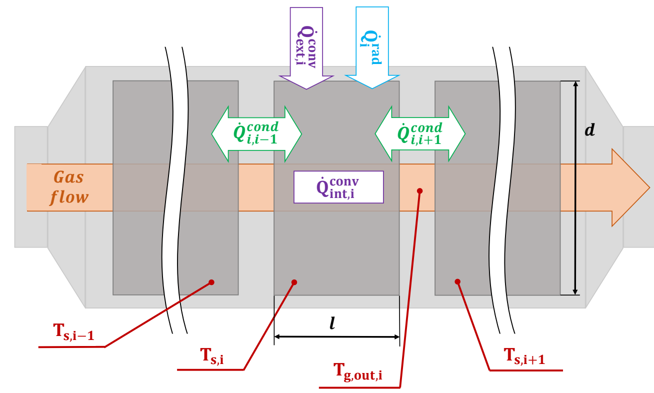

Figure 4 - Schematic representation of the thermal model used for EATS components, showing the representative temperatures and heat flows for the generic i-th brick.

More in detail, the thermal heat exchange with the exhaust gases is modeled for each device by dividing the physical component into a series of equivalent elementary bricks in which the contributions of conduction, radiation, external, and internal convection are calculated separately using semi-empirical formulas to determine the temperature of the solid material of the brick and of the exhaust gas at the brick outlet. The heat exchanged by internal convection $\dot{Q}^{conv}_{int,i}$ in one simulation time-step for the single i-th brick is given by the following equation:

$$\dot{Q}^{conv}_{int,i} = h_{int} \cdot A_{int} \cdot \left(T_{g,0,i} \frac{\epsilon_s}{1 + \frac{\epsilon_s}{\epsilon_t} - \epsilon_s} - T_{s,0,i} \frac{\epsilon_t}{1 + \frac{\epsilon_t}{\epsilon_s} - \epsilon_t} \right) \tag{1}$$

where A_{int} is the internal brick surface in contact with the gas, $T_{g,0,i}$ and $T_{s,0,i}$ are the initial temperatures of the gas and of the solid material respectively, while the parameters ϵ_s and ϵ_t are calculated for each brick as described in [35]. Finally, h_{int} is the convective heat transfer coefficient (HTC), obtained as:

$$h_{int} = \frac{Nu \cdot \lambda_g}{d} \tag{2}$$

being λ_g the thermal conductivity of the considered gas, d the diameter of the cross-section, and Nu the Nusselt number, calculated as a function of Reynolds number Re according to Meisner-Sorenson relation [36]:

$$Nu = 0.077 \cdot Re^{0.769} \tag{3}$$

The temperature of the gas at the brick outlet $T_{g,out,i}$ at the considered simulation time-step is calculated as:

$$T_{g,out,i} = T_{g,0,i} - Nu_t \cdot \left(T_{g,0,i} \frac{\epsilon_s}{1 + \frac{\epsilon_s}{\epsilon_t} - \epsilon_s} - T_{s,0,i} \frac{\epsilon_t}{1 + \frac{\epsilon_t}{\epsilon_s} - \epsilon_t} \right) \quad (4)$$

where Nu_t is the corrected Nusselt number, calculated as suggested in [37] to improve the model behavior during transients. The average temperature of the solid material $\overline{T}_{s,i}$, that is used to evaluate the other types of heat exchange, is obtained through the following equation:

$$\overline{T}_{s,i} = \overline{T}_{g,i} + \epsilon_t \cdot \left(T_{s,0,i} - \overline{T}_{g,i} \right) \quad (5)$$

where $\overline{T}_{g,i}$ is the average temperature of the gas crossing the brick, calculated as:

$$\overline{T}_{g,i} = \frac{T_{g,0,i} + T_{s,0,i} \cdot \left(\frac{\epsilon_t}{\epsilon_s} - \epsilon_t \right)}{1 + \frac{\epsilon_t}{\epsilon_s} - \epsilon_t} \quad (6)$$

The heat exchanged by external convection $\dot{Q}_{ext,i}^{conv}$ between the solid material of the brick and the surrounding environment for each simulation time-step is evaluated as follows:

$$\dot{Q}_{ext,i}^{conv} = h_{ext} \cdot A_{ext} \cdot \left(T_{amb} - \overline{T}_{s,i} \right) \quad (7)$$

where h_{ext} and A_{ext} represent the convective HTC and the heat transfer area respectively, while T_{amb} is the ambient temperature.

The contribution of radiation for the single brick $\dot{Q}_i^{rad}$ is calculated as:

$$\dot{Q}_i^{rad} = \sigma \cdot \epsilon \cdot A_{ext} \cdot \left(T_{amb}^4 - \overline{T}_{s,i}^4 \right) \quad (8)$$

where σ is the Stefan-Boltzmann constant and ϵ is the emissivity. The heat transferred by conduction $\dot{Q}_i^{cond}$ through the bricks is obtained through the following equation:

$$\dot{Q}_i^{cond} = \frac{\lambda_s \cdot A_{cond}}{l} \cdot \left(\overline{T}_{s,i-1} - 2\overline{T}_{s,i} + \overline{T}_{s,i+1} \right) \quad (9)$$

where λ_s is the thermal conductivity of the solid material of the brick, A_{cond} is the contact area between the bricks and l represents the length of the considered brick. Once all the contributions are calculated, the total heat flow $\dot{Q}_i^{tot}$ for the i-th brick for one simulation time-step is defined as:

$$\dot{Q}_i^{tot} = \dot{Q}_{int,i}^{conv} + \dot{Q}_{ext,i}^{conv} + \dot{Q}_i^{rad} + \dot{Q}_i^{cond} \quad (10)$$

which allows calculating the final temperature $T_{s,fin,i}$ of the solid material of the brick at the end of the simulation time-step:

$$T_{s,fin,i} = T_{s,0,i} + \frac{\dot{Q}_i^{tot}}{m \cdot c_p} \quad (11)$$

being m the mass of the considered solid material and c_p the corresponding specific heat capacity. The base architecture of the heat transfer model is the same for each component of the exhaust line (close-coupled and under-flow pipes included), adjusting all the coefficients for each specific component and taking into consideration also the contribution of any exothermic chemical process that may happen due to the conversion of pollutant species.

Since the attention of this paper is focused on NO_x emissions estimation, HC, CO, and soot emissions have been not taken into consideration for this analysis. Therefore, the exothermal reactions linked to the oxidation of these pollutant species, which would increase the exhaust gas temperature and thus improve the conversion efficiency of the SCR catalysts, are also neglected. Consequently, a conservative approach is adopted, and the worst case in terms of NO_x emission is considered. Focusing on NO_x reduction, the three main reactions which take place in the two SCR catalysts and in the SDPF are:

$$4\,NH_3 + 2\,NO + 2\,NO_2 \rightarrow 4\,N_2 + 6\,H_2O \quad (12)$$

$$4\,NH_3 + 4\,NO + O_2 \rightarrow 4\,N_2 + 6\,H_2O \quad (13)$$

$$4\,NH_3 + 3\,NO_2 \rightarrow \frac{7}{2}\,N_2 + 6\,H_2O \quad (14)$$

Reaction (12) is denoted as "fast SCR", while (13) and (14) are known as "standard SCR" and "slow SCR" respectively. The first reaction becomes very relevant if a high NO_2/NO_x ratio is provided, which happens if an oxidation catalyst is installed upstream the SCR catalyst (as for this specific application). The overall heat generated from NO_x reduction is evaluated by considering the specific enthalpy related to each of the previous chemical reactions and the moles of reduced NO_x. More in detail, being β the ratio between NO_2 and the total NO_x mass and M_{NO_x} the molar mass of the considered species, the moles of converted NO and NO_2 are obtained from the following equations:

$$n_{NO} = (1 - \beta)\, \frac{m_{NO_x}^{IN} - m_{NO_x}^{OUT}}{M_{NO}} \quad (15)$$

$$n_{NO_2} = \beta\, \frac{m_{NO_x}^{IN} - m_{NO_x}^{OUT}}{M_{NO_2}} \quad (16)$$

Then, the moles of NO and NO_2 involved in the "fast SCR" reaction are calculated as:

$$\min\left(n_{NO}, n_{NO_2}\right) = n_{NO}^{FAST} = n_{NO_2}^{FAST} = \frac{1}{2} n_{NH_3}^{FAST} = n_{FAST} \quad (17)$$

while the remaining moles of NO and NO_2 reacting in the "standard SCR" and "slow SCR" are:

$$n_{NO} - n_{NO}^{FAST} = n_{NO}^{STND} = n_{NH_3}^{STND} = n_{STND} \quad (18)$$

$$n_{NO_2} - n_{NO_2}^{FAST} = n_{NO_2}^{SLOW} = \frac{3}{4} n_{NH_3}^{SLOW} = n_{SLOW} \quad (19)$$

Finally, knowing the enthalpy of reaction h [J/mol] associated to each mole of reacting NO or NO_2, the overall heat resulting from NO_x reduction can be calculated as:

$$\dot{Q}_{exo} = \left(h_{FAST}\, n_{FAST} + h_{STND}\, n_{STND} + h_{SLOW}\, n_{SLOW} \right) \frac{1}{dt} \quad (20)$$

which is added to the total heat flow expressed by Equation (10) for the mentioned ATS components.

As already introduced, the EHC consists of one or more discs located upstream of the DOC that are heated by current flowing in high-resistance circuits. The exhaust gas flow is rapidly heated up before proceeding along the exhaust line, allowing fast heating that is independent of engine operation and extremely focused on the target devices. The electrical heater is modeled as one single brick, following the same equations already discussed above to calculate the temperature of the exhaust gas flow at the outlet. In this case, an additional contribution to the power balance is given by the electric power employed to heat the device and then transferred to the exhaust gas flow through internal convection.

2.2 Model validation

Since the described model is not representing an actual existing vehicle, a comprehensive vehicle model validation would not be possible due to the lack of experimental data. However, the adopted models for vehicle dynamics, electric power unit, internal combustion engine, and after-treatment system have been individually validated as part of previous research activities. Accordingly, a comparison between simulated and experimental results of the most significant quantities involving ICE and EATS operation is shown in the following paragraphs.

The validations of vehicle dynamics, EM, and HV battery models are not fully presented within this work since it goes beyond the purpose of this activity. However, a detailed description of the test cases and conditions considered for the mentioned validation can be found in [34].

The map-based ICE and EATS models have been calibrated and validated within previous activities carried out by FEV, comparing simulation results with measured data collected during steady state and dynamic tests on the chassis dynamometer. Figure 5a shows a good match between the simulated and the experimental trend of both ICE brake mean effective pressure (BMEP) and rotational speed. Moreover, according to the instantaneous and cumulated CO_2 profiles, even if some experimental CO_2 peaks are not perfectly captured, the transient behavior is balanced over the whole driving cycle so that the total estimated CO_2 emissions are in good agreement with the experimental values. The same applies also to raw NO_x emissions estimation (Figure 5b).

Concerning the EATS model, a modular approach was adopted, so that the same modeled blocks representing every single component can be possibly combined to build several different EATS layouts depending on the specific application. Although experimental data, and thus direct validation, are not available for the proposed EATS layout, the validation of each single component can be derived as part of different EATS layouts that have been tested and experimentally characterized. Accordingly, the comparison between simulated and experimental data related to two different EATS layouts is provided in Figure 6. As already mentioned, according to the purpose of this paper, the attention has been focused on NO_x emissions estimation. In this regard, Figure 6 shows a good matching between simulated and experimental data in terms of engine-out (EO) and tailpipe (TP) cumulated emissions, despite some inaccuracies concerning instantaneous quantities.

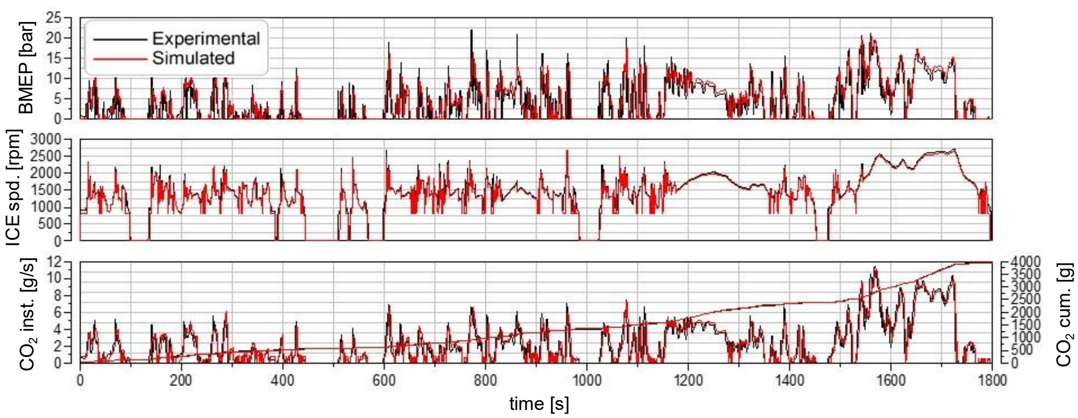

(a)

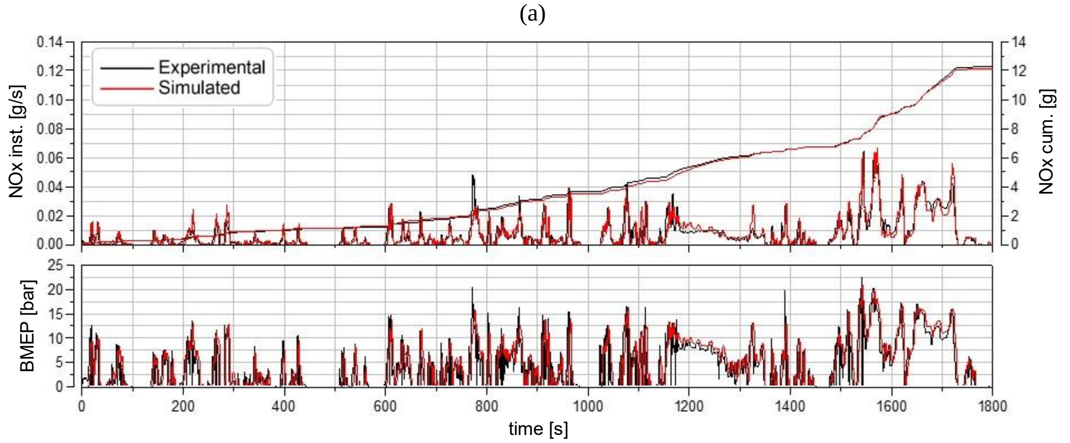

(b)

*Figure 5 - ICE (**a**) and emission (**b**) model validation: experimental (black) and simulated (red) results over a Worldwide harmonized Light vehicles Test Cycle (WLTC).*

Since experimental data were not available for the electrical heater, a different type of validation has been proposed: output data coming from an electrical-heater validated model already available from GT-power® libraries have been used as a reference and compared with the ones provided by the considered Simulink® model. The same input data in terms of air mass flow, electrical power, and inlet temperature are supplied to both simulation platforms and exhaust gas temperature values at the e-heater outlet are then compared (Figure 7). Although some inaccuracies can be noticed especially during fast transients, the two sets of data follow the same general trend, which is considered acceptable for the scope of this application.

To summarize, with the adopted simulation approach, a realistic estimation of CO_2, engine-out pollutant emissions, EATS behavior, and thus NO_x tailpipe emissions is given. This level of accuracy is acceptable for the purpose of this activity, which is to highlight the potential of a predictive control strategy paired with a possible state-of-the-art PHEV+EATS system in terms of NO_x emissions reduction.

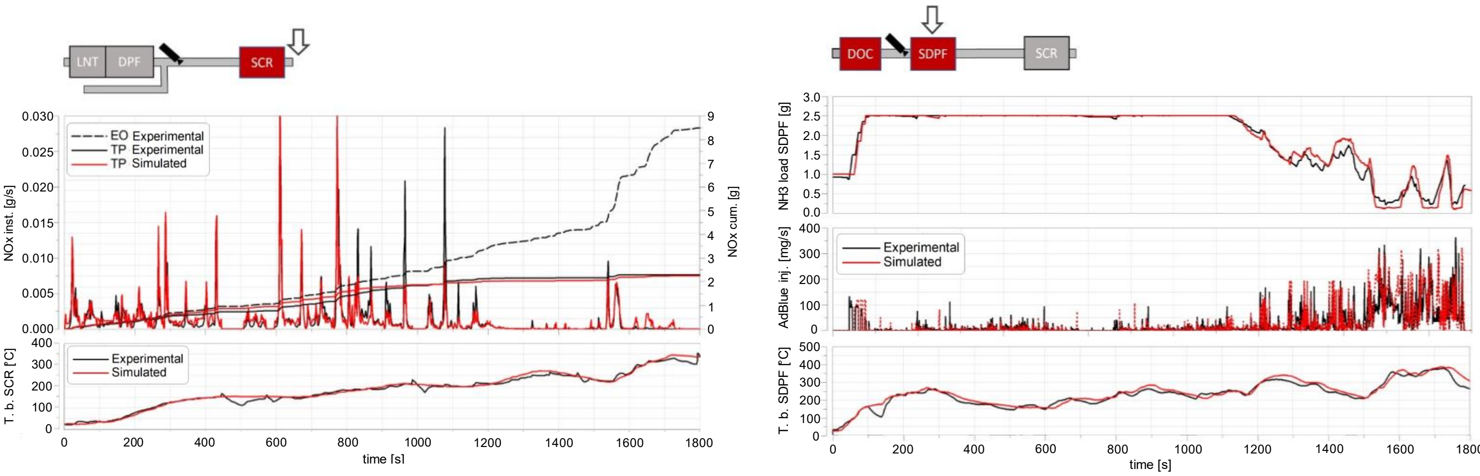

(a) (b)

*Figure 6 - EATS components model validation: experimental (black) and simulated (red) results over a WLTC. A schematic representation of the specific tested layout, including LNT, DPF, and SCR in the first case (**a**) and DOC, SDPF, and SCR in the second case (**b**). Measurement locations of NOx emission (case (**a**)) and injected AdBlue (case (**b**)) are provided by the white arrows.*

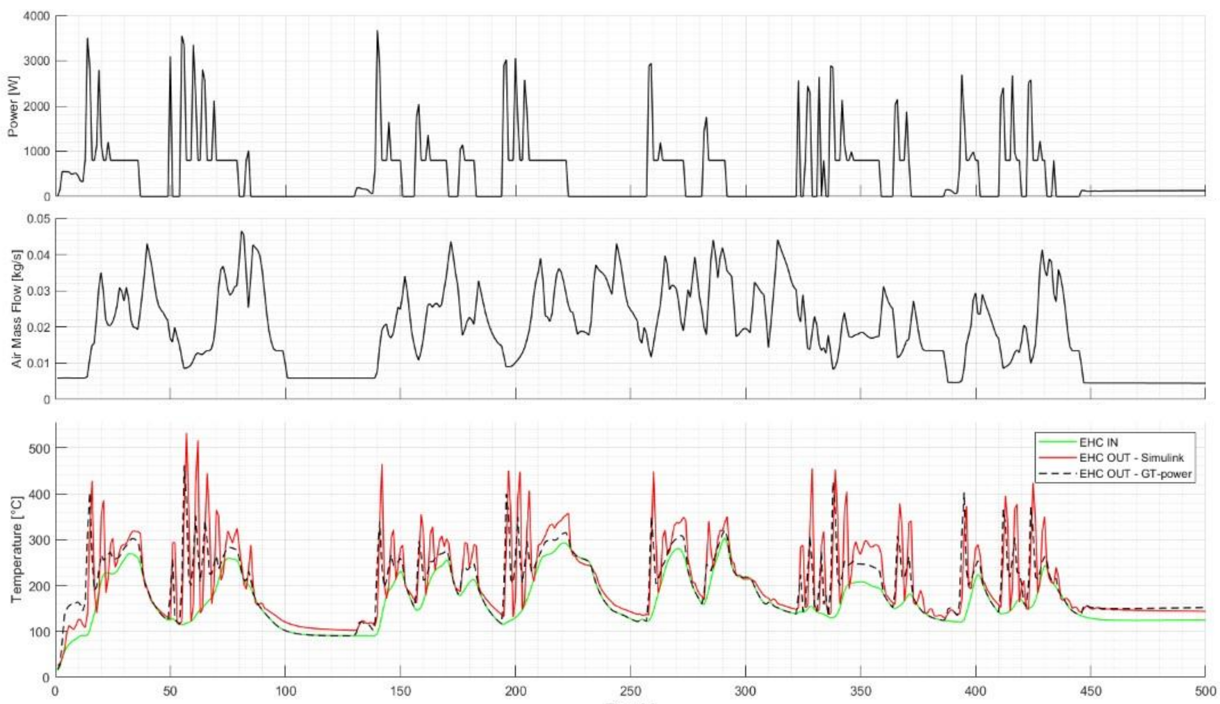

Figure 7 - E-heater model validation: exhaust gas temperature at e-heater outlet from GT-power® (black dashed) and Simulink® (red solid) for the same input data (black solid and green solid

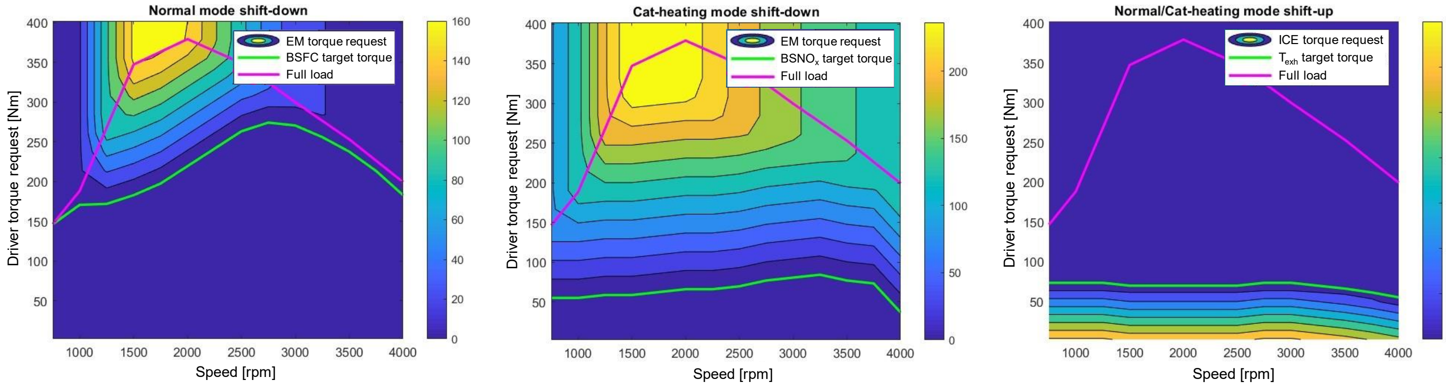

(**a**) (**b**) (**c**)

2.3 Torque split strategy

The development and calibration of a robust and effective hybrid control strategy is a preliminary step for the implementation of additional control functions involving EATS thermal management. The selection of the driving mode between full electric drive (e-drive) and hybrid drive relies on a set of logical conditions implemented in the vehicle HCU (Hybrid Control Unit). These conditions consider several parameters involving driver torque request, actual vehicle speed, HV battery SoC and EATS temperature. More in detail, torque and speed thresholds to switch from full electric to hybrid driving mode have been set according to EM operating limits. A HV battery SoC constant threshold and related hysteresis have been set through a DoE approach to minimize weighted CO_2 emission on a complete WLTP standard procedure (see Appendix A, *Figure A 3*). A further condition on DOC temperature has been introduced to promote EATS heating up after engine cold start, avoiding ICE switch-off if DOC temperature is below the light-off value. Finally, a minimum threshold for ICE operating time has been set to prevent too frequent ICE starts and stops that would affect vehicle drivability. All the mentioned logical conditions are summarized in *Table 3*.

Table 3 - Set of logical conditions enabling the switch from e-drive to hybrid drive and vice-versa.

Parameter	**Condition to switch to hybrid mode**	**Condition to switch to e-drive**
Vehicle speed	> 140 km/h	< 130 km/h
Driver torque request	> EM max. continuous torque*	< EM max. continuous torque*
HV battery SoC	< 18%	> 20%
DOC temperature	-	> 180°C
ICE operating time	ICE off time > 2 s	ICE on time > 10 s

*Continuous torque, rather than peak torque, is considered to always keep a torque reserve for the ICE start.

Focusing on hybrid mode, the torque split between ICE and EM is managed using a map-based approach. Three different load point shift (LPS) maps have been generated following different targets in terms of BSFC (Brake Specific Fuel Consumption), BSNOx (Brake Specific NOx emission) and engine-out exhaust gas temperature depending on ICE operating conditions. These targets have been set through a DoE process aimed to find the best trade-off in terms of NOx emission and fuel consumption on a WLTC driving cycle performed in CS mode. For the sake of brevity, LPS maps resulting from this calibration process have been collected and described in Appendix A (

).

As a common feature of PHEVs, the overall behaviour of the adopted hybrid control strategy can be defined as charge depleting – charge sustaining (CD-CS), aiming at driving in pure electric mode as much as possible (CD phase) and requesting ICE start switching to the hybrid mode only if strictly necessary (CS phase). In hybrid mode, the torque split is managed following different targets of BSFC and NO_x emissions depending on the specific operating conditions while the SoC is kept in the range between 18% and 20%, avoiding too low SoC values that would damage the battery.

2.4 Development of EHC predictive control function

As already mentioned in section 1, the availability of real-time navigation data, sent to the vehicle by a map-service provider, allows the reconstruction of the future driving scenario (eHorizon), thus enabling the development of predictive control strategies aimed to the optimization of energy management and pollutant emissions. For a (P)HEV, the knowledge of future driving conditions can also be used to predict ICE first start along the travelled route, which is a key enabler for the predictive thermal management of the EATS. In fact, it allows to perform a pre-heating phase that can be planned to avoid NO_x cold start emissions, which significantly contribute to the total emissions along the considered driving cycle.

2.4.1 Pre-heating strategy definition

A preliminary step for the development of an effective EHC control strategy is to determine the heating power needed to heat up the EATS for achieving the desired conversion efficiency. In this regard, several simulations have been performed to evaluate the effects related to different values of provided electrical power and air flow rate on DOC, LTM-SCR, SDPF and SCR light-off time. More in detail, constant heating power and secondary air flow rate have been provided with engine off to evaluate the only effect of EHC on EATS heating dynamics. Then, the time needed to reach the light-off temperature, considered as the threshold above which the pollutants conversion efficiency of each after-treatment device reaches its maximum asymptotic value (180°C for the DOC and 220°C for the SCR catalysts, according to the respective pollutant conversion efficiencies maps), has been evaluated for the mentioned devices. The results, graphically represented in Figure *8*, clearly point out that the light-off time of all the devices decreases with increasing power and air flow rate so that the same result can be achieved with different combinations of the considered parameters. It can be also noticed that the light-off temperature cannot be reached at all below a minimum threshold of secondary air flow rate and heating power, especially referring to the SCR catalyst (Figure 8d).

Starting from these considerations, different pre-heating strategies providing increasing heating power and secondary air flow rate have been tested to find the most convenient pre-heating strategy in terms of resulting NO_x emissions and energy consumption. As pointed out by the previous results, the light-off of the DOC (Figure 8a) and especially of the LTM-SCR (Figure 8b) cannot be achieved in a reasonable time for values below 2 kW and 20 kg/h of EHC power and secondary air flow rate respectively.

Therefore, according to the technical specifications of secondary air pumps and EHCs available on the market for Diesel applications, a range between 2 and 4 kW for the heating power and between 20 and 55 kg/h for the secondary air flow rate has been considered for the following analysis, as summarized in Table 4.

Table 4 - Pre-heating strategy definition: tested and final configurations.

Parameter	Tested range	Final configuration
EHC power [kW]	2 ÷ 4	4
Secondary air flow [kg/s]	20 ÷ 55	55
Pre-heating time [s]	0 ÷ 200	60

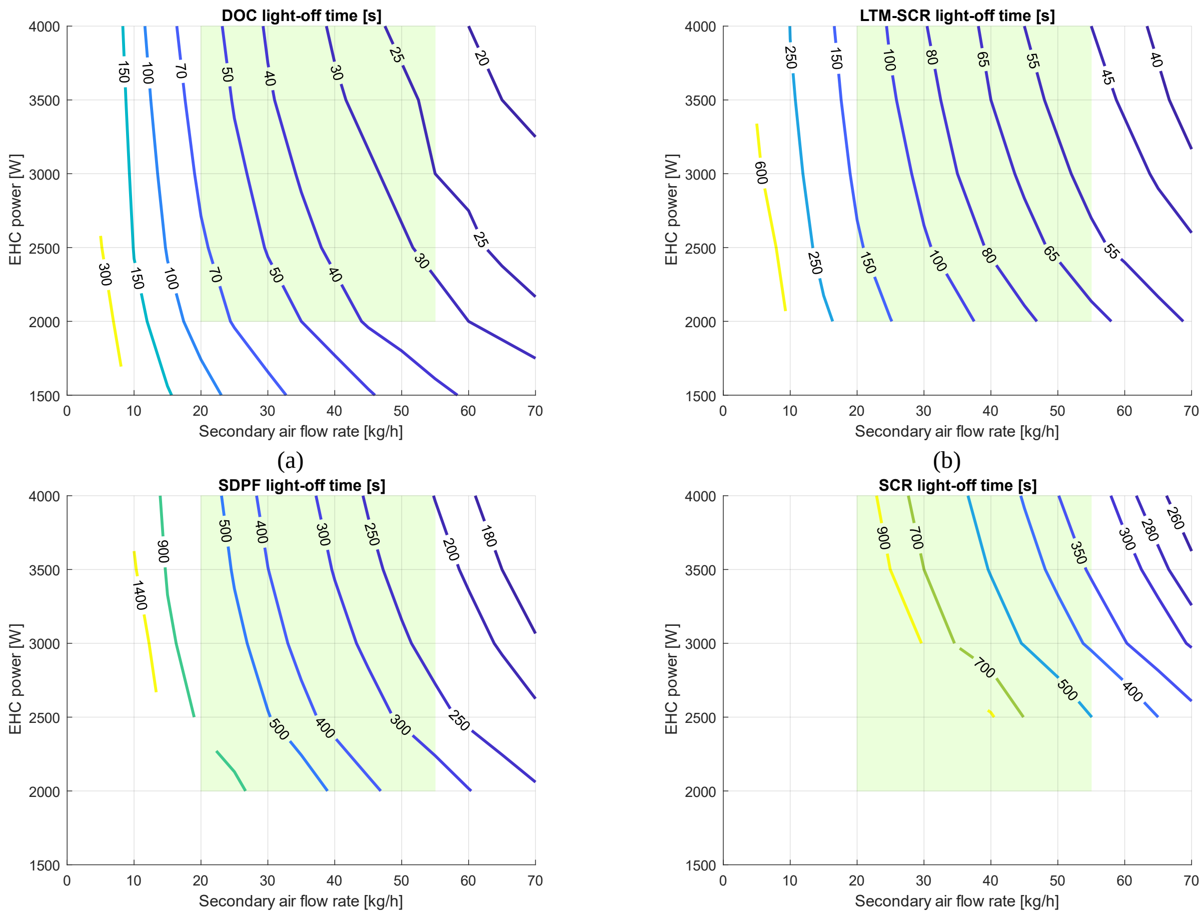

*Figure 8 - DOC (**a**), LTM-SCR (**b**), SDPF (**c**) and SCR (**d**) light-off time as a function of secondary air flow rate and EHC power. The green area highlights the feasible range of power and secondary air flow taken into consideration for the pre-heating strategy definition, according to section 2.4.*

Each different configuration has been tested on a real-diving emissions (RDE) cycle with increasing pre-heating time. The initial state of charge (SoC) has been set to 22% arbitrarily to force ICE start along the considered driving cycle.

As expected, the best results in terms of absolute NO_x cumulative emissions are achieved with the highest heating power and air flow rate. Based on this consideration, from this point on the analysis has been focused on the configurations adopting the maximum air flow rate and heating power that can be actually provided. Relative emissions are calculated as the ratio between the absolute cumulative emissions resulting from the considered pre-heating strategy and the one obtained with no pre-heating along the same driving cycle. As it can be noticed in Figure 9a, the trend of NO_x reduction gets less steep as the pre-heating time increases, until reaching an asymptotic value, which is significantly higher for the lower value of EHC power due to the limited temperatures that can be reached in these conditions. On the other hand, the CO_2 trend, shown in Figure 9b, is increasing with the pre-heating time, due to the higher energy consumption that is compensated by increased use of the ICE to keep the SoC above the lower threshold. In addition, a CO_2 emission reduction is observed for a limited range of pre-heating duration with respect to the base strategy with no pre-heating, despite the additional energy consumption requested in the first case. This is because, according to the adopted strategy which has not been described within this work for the sake of brevity, after the first start the ICE can be switched off again only when the DOC light-off is achieved.

Thus, the engine is forced to run for longer time if no pre-heating is planned, due to lower temperature of the EATS, and this completely deletes the advantage in terms of CO_2 reduction related to the energy saved if no pre-heating takes place. Beyond this additional consideration, according to the purpose of this activity, the pre-heating duration has been set to 60 seconds, to provide a result in terms of NO_x reduction that is close to the asymptotic one but that at the same time leads to a limited CO_2 increase duration the gain in terms of NO_x reduction becomes less attractive considering the related cost in terms of CO_2 emission.

2.4.2 Engine start prediction

Since the chosen application is a PHEV, it is reasonable to assume that in standard conditions the vehicle will start each driving cycle in full electric mode. Then, the vehicle hybrid control unit (HCU) asks for ICE start and manages the torque split between ICE and EM according to a calibrated rule-based strategy depending on SoC, ICE and EATS operating conditions. Starting from this assumption, as already introduced in section 1, the prediction of engine first start is the key enabler for the development of the described EHC predictive control strategy. In this regard, a simplified and thus faster backward vehicle model (BVM) has been implemented in the HCU, allowing to estimate the trend of all the relevant quantities, with particular reference to EM torque request and HV battery SoC. A detailed description of the

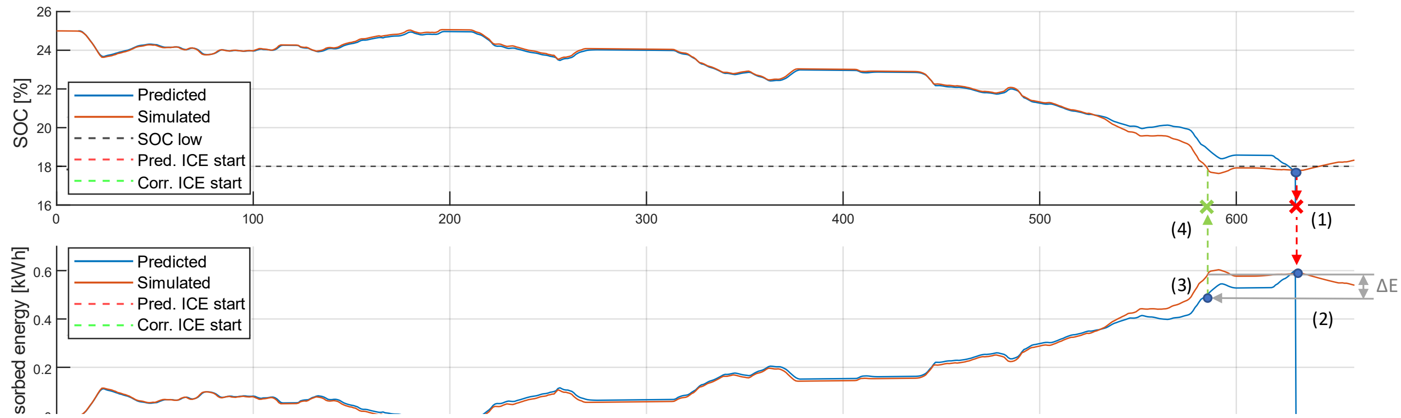

Figure 10 - Predicted and actual HV battery state of charge (top) and corresponding adsorbed energy (bottom) along an RDE urban cycle with 25% initial SoC. According to the adopted convention, a positive gradient in the energy curve corresponds to battery discharging, while a negative gradient to battery charging.

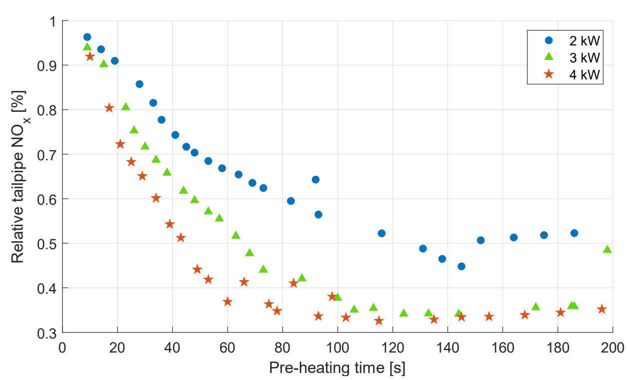

(a)

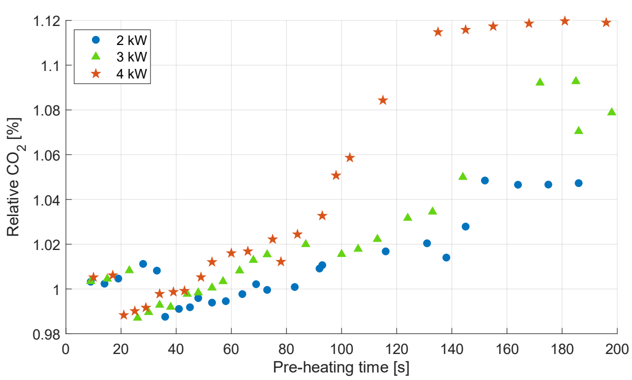

(b)

mentioned model can be found in [24]. Since this paper is focused on quantifying the benefits introduced by an EHC predictive function on NO_x emissions reduction, navigation data, such as vehicle speed and road slope profile, which are the inputs to the BVM, are assumed to be

*Figure 9 - Relative tailpipe NO_x (**a**) and CO_2 (**b**) emission for variable EHC power and pre-heating time for fixed air flow rate of 55 kg/h.*

known a priori. Due to the different powertrain layout with respect to the one described in [20], a simplified transmission model has been added, which calculates the gear profile based on the same rule-based shifting strategy implemented in the HCU subsystem responsible for the gear shifting. Since the aim is to predict the engine first start, e-drive is the only driving mode considered within the prediction, so that once known the selected gear, EM torque request can be easily derived from the total torque request. Starting from the power request, a simplified HV battery model allows calculating the SoC trend.The prediction of vehicle speed profile, engine torque request and SoC trend, coming from the BVM, is the input for a dedicated function that has been developed and implemented in the HCU model to predict engine first start, which can be derived based on the same conditions for e-drive or hybrid drive selection already implemented in the HCU. More in detail, the output of this function is the time instant in which the engine start is expected to be requested, namely when at least one of the following conditions is true:

- Predicted vehicle speed above 140 km/h;
- Predicted EM torque request beyond the continuous torque available from motor specification at the considered speed;
- Predicted SoC lower than 18 %.

However, the so obtained engine start prediction instant does not consider the additional energy consumption coming from EHC and secondary air pump during the EATS pre-heating phase. This is because the pre-heating phase is planned subsequently based on the ICE start prediction itself. Due to this, a significant error is introduced in the SoC trend prediction, which becomes an issue if ICE start is driven by the condition related to low SoC, leading to an inaccuracy in the engine start prediction that cannot be neglected for the purposes of this activity. For this reason, a correction has been applied to the prediction to overcome this issue. The additional energy ΔE needed to perform the pre-heating phase is calculated based on the requested power $P_{PreHeat}$ and heating time $\Delta T_{PreHeat}$ that have been previously set:

$$\Delta E = P_{PreHeat}\,\Delta T_{PreHeat} \tag{21}$$

This amount of energy is then subtracted from the energy available in the HV battery to identify the correct time instant in which the SoC will drop below the selected threshold determining the ICE start request.

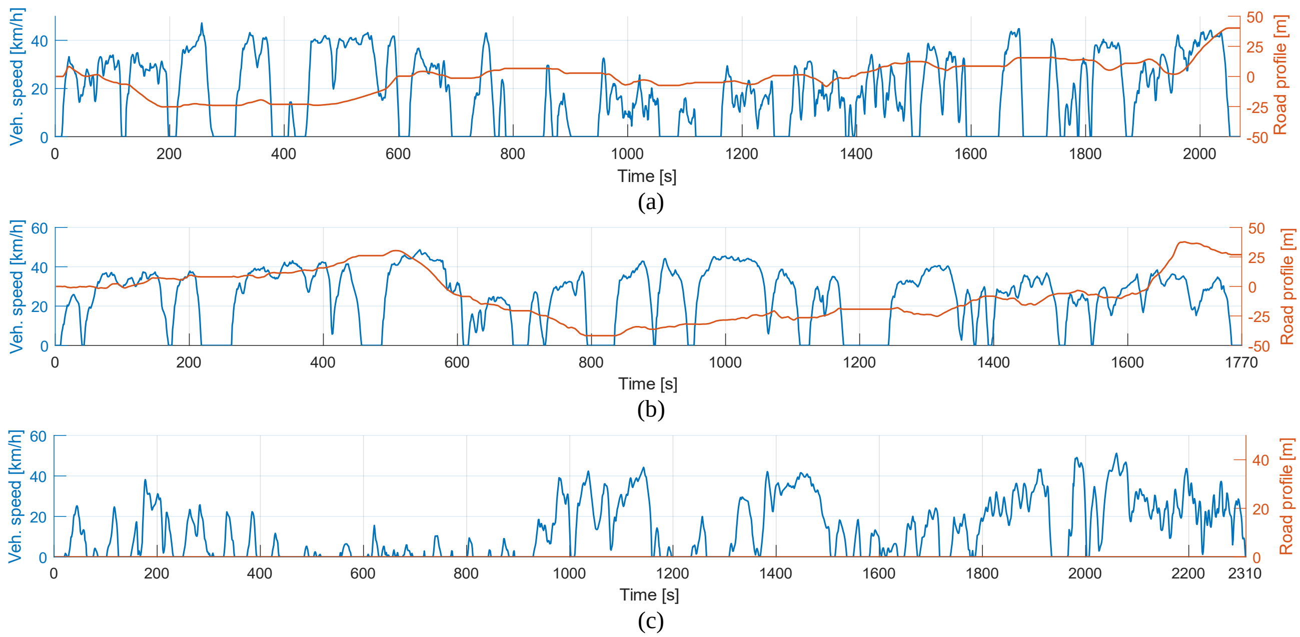

For the sake of clarity, the top plot of **Errore. L'origine riferimento non è stata trovata.** shows a comparison between the predicted SoC trajectory (not corrected) and the simulated one (resulting from the application of the predictive strategy) along the first part of an RDE urban cycle starting with very low SoC. As it can be seen, in the first 500 seconds of the cycle the two traces are almost coincident except for a slight offset due to natural inaccuracies of the predictive backward model. Then a significant deviation between the two trends can be noticed when the pre-heating phase starts, based on the prediction itself. The additional energy request leads to a faster decrease of the actual SoC, thus causing the actual ICE start to happen in advance with respect to the prediction. Therefore, if a correction is not applied, this would lead to a shorter heating phase with respect to the planned one. Therefore, the focus is shifted to the prediction of the

Figure 11 - Vehicle speed (blue) and slope (red) profiles of the simulated urban driving cycles: RDE 1 (a), RDE 2 (b), and RDE 3 (c)

energy absorbed by the HV battery, shown at the bottom of **Errore. L'origine riferimento non è stata trovata.**: starting from the time instant corresponding to the predicted engine start (1), the amount of energy ΔE absorbed during the pre-heating (2) is subtracted to the prediction of the total energy provided by the battery until that moment (3); finally the time instant related to the so obtained energy value corresponds to the actual ICE start if the pre-heating energy had been taken into consideration, referred to as corrected ICE start (4).

Table 5 - ICE start prediction evaluation over different driving cycles and initial HV battery SoC.

Cycle	Initial SoC [%]	Predicted ICE start [s]	Corrected ICE start [s]	Actual ICE start [s]
WLTC	22	502	452	453
	25	677	612	615
	30	1416	1347	1350
RDE 1*	22	279	251	253
	25	636	584	584
	30	855	839	843
RDE 3*	22	1003	916	917
	25	1451	1372	1373

*These driving cycles will be introduced and fully described in section 2.5.

The effectiveness of the performed correction is tested over different driving cycles starting with different initial SoCs. The results, summarized in Table 5, prove that in most cases the introduced correction allows to significantly reduce the gap between predicted and actual engine start, which was the main target, even if a residual error is still present due to inevitable inaccuracies of the simplified backward model implemented in the HCU. Finally, the output signal carrying the information about the time instant corresponding to the predicted engine start, which is calculated by the HCU in the first few seconds of driving, is sent to the engine controller, which is responsible for the management of the EHC and the secondary air pump. Based on this information, the pre-heating phase is planned using a timer, according to the pre-heating time that has been set for the defined pre-heating strategy. The pre-heating phase automatically stops when the engine is switched on and from that moment a rule-based strategy (RBS) manages the EHC power request by means of a PI controller to ensure a minimum target temperature of the exhaust gases providing the maximum conversion efficiency of the DOC and LTM-SCR. The significant gain achieved in terms of NO_x emissions reduction by considering an EHC predictive control strategy (PS), which differs from the reference RBS by the introduction of a pre-heating phase, is presented in section 0.

Looking to an undesiderable but still possible situation in which realiable eHorizon data were temporarily unavailable, EATS pre-heating is managed following a rule-based approach. According to this "fallback strategy", the pre-heating starts when the SoC falls below 20%, assuming that in a short time it will decrease even more reaching the lower threshold of 18%, so that the HCU will request the engine start. However, unlike what happens considering the predictive strategy, in this case the period between EHC activation and the engine start can significantly vary depending on the specific driving conditions; so, once the target EATS temperature is reached, then the EHC power is managed by the same PI controller that has been previously introduced, in order to keep the EATS temperature around the target until the engine start. Of course, most of the times, this strategy is far from the optimum and shows many drawbacks if compared to the predictive one: in fact, it may happen that the pre-heating gets shorter than the planned one if the SoC drops very quickly below the lower threshold, leading to higher pollutant emissions if the EATS temperature has not yet reached the target value when the engine is turned on. On the other hand, it may happen that the pre-heating gets much longer than the planned one if the power requested to the EM is low and the SoC decreases slowly, leading to a significant energy waste due to the extended EHC power supply. Moreover, as a further limitation, the fallback strategy does not take into account ICE starts due to high torque request or high vehicle speed, being characterized by much faster dynamics which are hard to be controlled through a simple rule-based strategy which does not rely on predictive information. For the sake of brevity, and since it goes out of the scope of this paper, the results related to this fallback strategy are not included in the next sections.

2.5 Test cases and conditions

Different real driving scenarios have been considered to test the proposed EHC control strategy and highlight its benefits in terms of NO_x emissions reduction. In particular, three urban driving cycles, listed in **Errore. L'origine riferimento non è stata trovata.**, have been selected in order to provide challenging conditions from the point of view of NO_x emission, being characterized by frequent start and stop phases and, on average, by engine low load operation, which results in lower temperatures of the EATS. The vehicle speed profile and road slope of the considered driving cycles are shown in **Errore. L'origine riferimento non è stata trovata.**. The initial battery SoC for each simulation has been varied between 22% and 30% to force ICE start within the driving cycle. The improvement achieved thanks to the introduction of an EATS pre-heating phase based on ICE start prediction will be evaluated considering EATS components temperature profile over time and the resulting average NO_x emissions along each considered cycle. This type of test is in line with the expected Euro 7 regulations, which will consider nearly any possible driving scenario, as already introduced in section 1.

Table 6 - Simulated driving cycles and relevant features.

		RDE 1	RDE 2	RDE 3
Duration	[s]	2070	1770	2310
Distance	[m]	10510	12219	8467
Perc. stop	[%]	27	17.1	31.7
Max. speed	[km/h]	47.2	48.6	51.2
Avg. speed*	[km/h]	25.0	30.0	19.3
Max. acc.	[m/s^2]	3.50	3.16	3.42

*The calculated average speed does not consider vehicle stops.

In this context, a comparison with the Euro 7 NO_x estimated emission limits will be provided. In particular, according to [31], two possible scenarios are considered: a less demanding "Scenario A", which would set the NO_x emissions limit to 30 mg/km, and a more demanding "Scenario B", which would lower this limit to 10 mg/km. The same ambient temperature, set to 25°C, has been considered for all the test cases, since the effect of variable environmental conditions on the resulting CO_2 and NO_x emissions has not been investigated in this work.

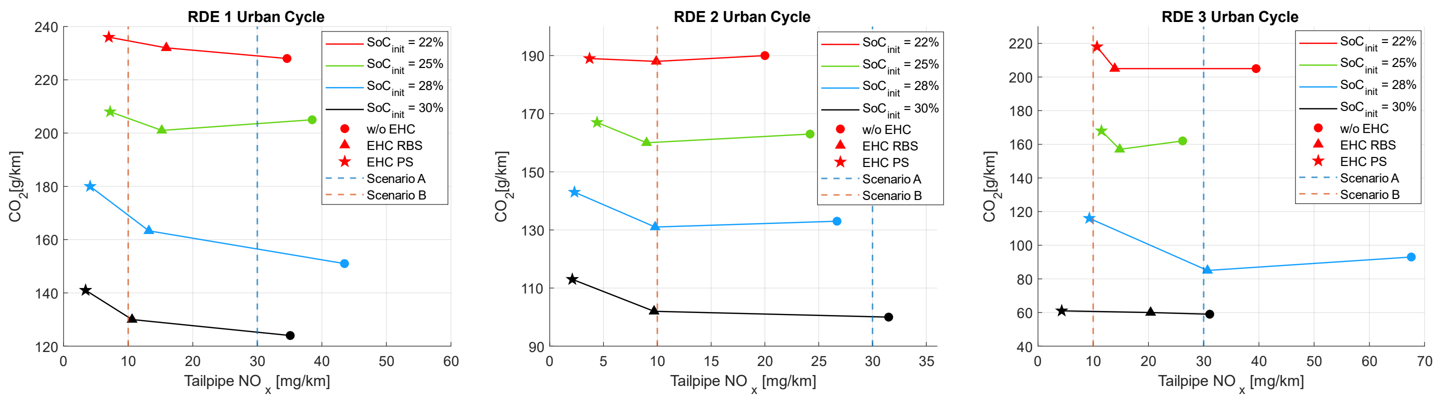

(**a**) (**b**) (**c**)

Figure 12 - Comparison between the proposed predictive EHC strategy, the EHC rule-based strategy, and the same strategy with no EHC usage: resulting average NOx and corresponding CO2 emissions for different urban driving cycles with variable initial SoC (SoCinit).

3 Results and discussion

The results in terms of tailpipe NO_x and CO_2 emissions along the three considered urban driving cycles are summarized in **Errore. L'origine riferimento non è stata trovata.**. In particular, the comparison between the rule-based EHC control strategy ("EHC RBS") and the proposed predictive control strategy ("EHC PS") highlights that a significant additional reduction of average NO_x emission along the considered driving cycles is achieved thanks to the introduction of an EATS pre-heating phase. The results related to the same application with no EHC usage ("w/o EHC") are included for completeness. Focusing on plot (**c**) of **Errore. L'origine riferimento non è stata trovata.**, it can be noticed that the data referred to the cases "w/o EHC" and "EHC RBS" with 28% initial SoC show abnormal behavior, with significantly higher NO_x emissions if compared to the general trend. This is due to a very high peak in the engine-out emissions which is well managed by the PS strategy thanks to the pre-heating phase and the earlier ICE start with respect to the other two cases, in which the ICE start occurs much closer to the mentioned peak of engine-out NO_x emissions and no pre-heating takes place, thus resulting in very low EATS temperatures and conversion efficiencies.

As expected, the overall CO_2 trend is significantly increasing with decreasing initial SoC, due to a shorter e-drive range, and slightly increasing switching from the "EHC RBS" to the predictive one, which includes an EATS pre-heating phase and thus significant additional energy consumption, which is compensated by greater use of the engine to recharge the battery. On the other hand, comparing the cases without EHC and the "EHC RBS", as for the previous comparison, we would expect higher CO_2 emissions for the "EHC RBS" due to the EHC electric consumption. However, the CO_2 trend is not the same for all the cases, which can be explained by considering the different factors that come into play. In some cases, this behavior can be simply explained by considering that the final SoC could be slightly different from one case to the other, thus leading to a higher final CO_2 emission if a higher final SoC is reached, meaning that more power has been provided by the ICE, either for traction or to recharge the battery. In parallel, as described in 2.3, the hybrid strategy is strongly affected by EATS temperature: the ICE is forced to run until a minimum temperature of the DOC is reached, which takes a longer time if the contribution of the EHC is not considered, thus delaying the switch to the e-drive mode even if the upper SoC threshold has been already reached. Depending on the driving cycle, this could force the engine to run in inefficient operating points in which in normal conditions, namely when the cat-heating phase has been completed, it would have been switched off, leading to higher fuel consumption. Moreover, the ATS temperature has an impact on the choice of the LPS maps to be used as well (Appendix A, *Hybrid strategy: LPS maps*): when the EATS temperature is above the lower threshold, the LPS map used for the torque split during EM boosting is set to operate the engine following the target BSFC; during cat-heating, a different LPS map is used, with the aim of limiting engine-out NO_x emission by reducing the engine load, which, on the other hand, results in higher BSFC due to lower engine efficiency. These considerations, combined with the previous ones related to the final SoC values and the presence of some specific maneuvers reflecting the randomness of the cycle, fully explain the different behaviors of the considered cases in terms of CO_2 emissions. For the sake of brevity, and since it goes outside the scope of this paper, the values of final SoC and average BSFC for all the cases have not been included in this work.

To highlight the benefits in terms of NO_x emissions reduction given by the introduction of an EATS pre-heating phase based on engine start prediction, the attention is now focused on the comparison between RBS and PS. Three cases among those simulated are deeper analyzed in the following section as representative of possible different situations that can be encountered, based on all the observed cases:

1. RDE 1 urban cycle with 25% initial SoC;
2. RDE 3 urban cycle with 25% initial SoC;
3. RDE 3 urban cycle with 30% initial SoC.

3.1 Case 1

In this case, the first ICE start is determined by the minimum SoC condition, and it is correctly predicted by the HCU (Figure 13 and Figure 14), allowing to perform the planned pre-heating phase. The exhaust gas temperature profiles at LTM-SCR, SDPF, and SCR outlet obtained with the two different strategies are shown in Figure 15, together with EHC requested power and the resulting tailpipe NO_x emissions. It can be noticed that almost 60% of the total NO_x are emitted within 200 seconds after the first ICE start. Therefore, the gain obtained with the introduction of a pre-heating phase is significant, allowing to heat up in advance the two SCR catalysts and reduce the average tailpipe NO_x emissions along the driving cycle by more than 50%, from 15.2 mg/km to 7.2 mg/km, although engine-out emissions are almost the same.

3.2 Case 2

As for case 1, the first ICE start is determined by the SoC-related condition and it is correctly predicted by the HCU, as shown in Figure 16 and Figure 17. However, despite the pre-heating phase, a higher NO_x emission is observed for the predictive strategy during the first ICE start, as pointed out by Figure 18: in this case, immediately after the ICE start, there is accidentally a peak in the driver torque request (Figure 17). This results in a peak of engine-out NO_x emissions and therefore higher tailpipe emissions with respect to the case in which the rule-based strategy is applied, despite the higher EATS temperature and conversion efficiency provided by the EHC predictive strategy. Anyway, the pre-heating phase, thanks to the higher temperature reached by the SDPF and the SCR catalyst in particular, allows to limit NO_x tailpipe emission for the last part of the cycle, thus compensating the higher emission resulting from the first ICE start. Consequently, the average NO_x emission along the whole driving cycle results still 20% lower for the predictive approach (11.5 mg/km with respect to 14.8 mg/km resulting from the “EHC RBS”), showing the effectiveness of this strategy in limiting the final tailpipe emissions, despite the much more demanding situations that may be realistically encountered and thus higher engine-out emissions. The same considerations can justify the similar trend of NO_x reduction shown by the test case performed on the same driving cycle but with 22% initial SoC.

3.3 Case 3

In this case, the first ICE start is determined by the condition related to the EM torque limit and it is correctly predicted by the HCU, as proven by Figure 19, which compares the actual and predicted trend of EM torque request together with the corresponding EM torque limits in the last 500 seconds of the considered driving cycle. As for the other cases, the higher temperature reached by the EATS thanks to the planned pre-heating phase allows to strongly reduce NO_x emissions due to ICE first start (

), which in this case are responsible for almost 70% of the final tailpipe emissions. Therefore, due to the high impact of ICE first start on the total emissions, a very significant percentage reduction, which is close to 80%, in the average tailpipe NO_x emission is observed, moving from 20.4 mg/km for the “EHC RBS” to 4.3 mg/km for the “EHC PS”.

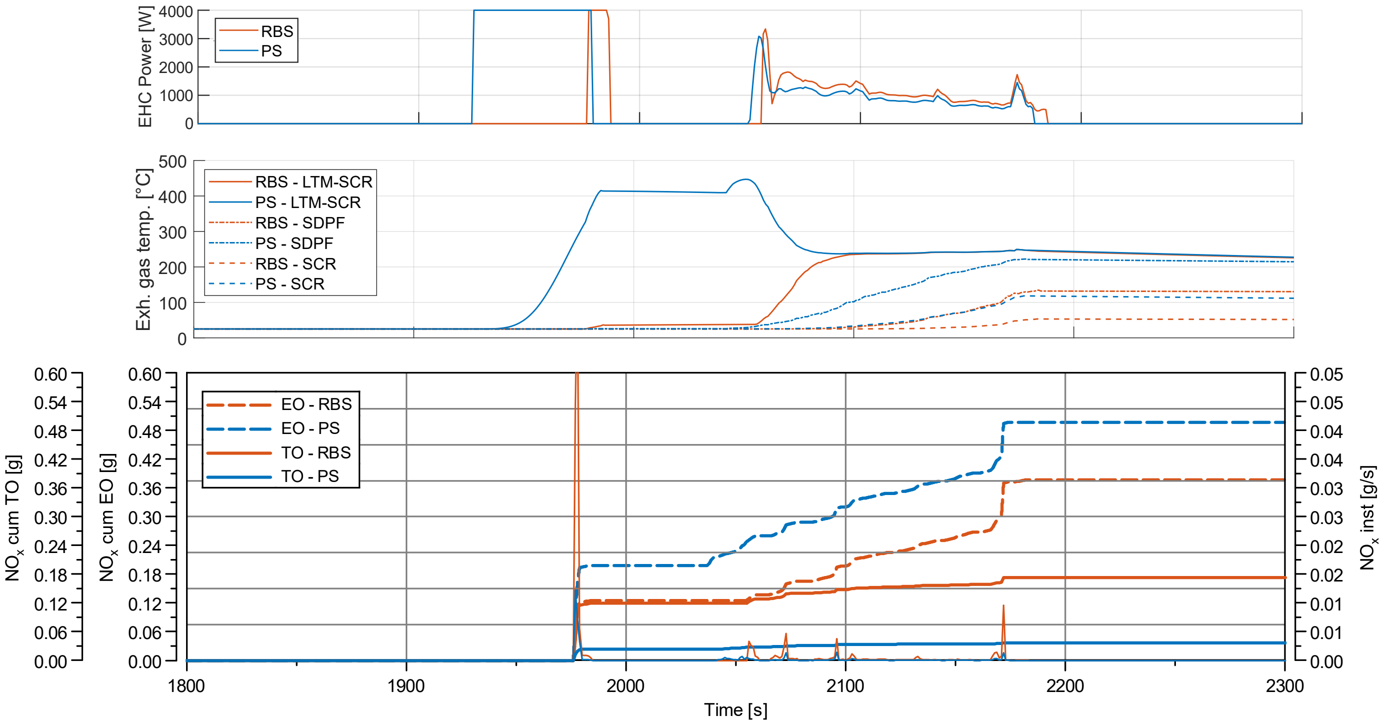

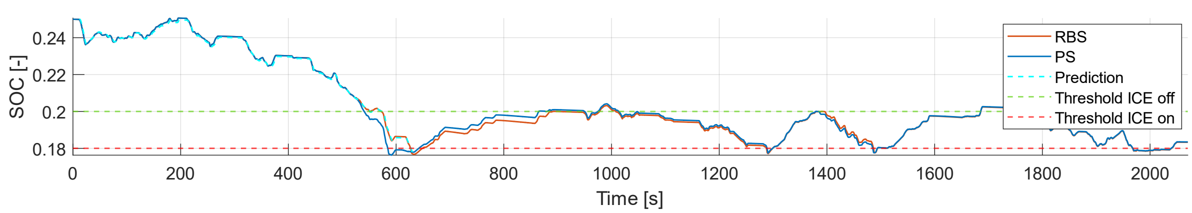

Figure 13 - Case 1: comparison of SoC traces for rule-based (red) and predictive (blue) EHC control strategies; cyan dashed line shows the SoC trace prediction. Lower and upper SoC thresholds below and above which ICE is turned on or off respectively are shown as well.

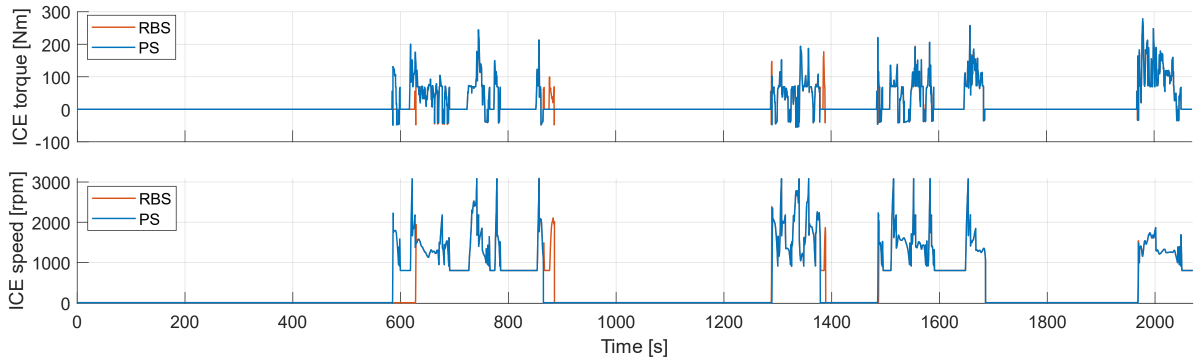

Figure 14 - Case 1: comparison of ICE speed and torque for rule-based (red) and predictive (blue) EHC control strategies.

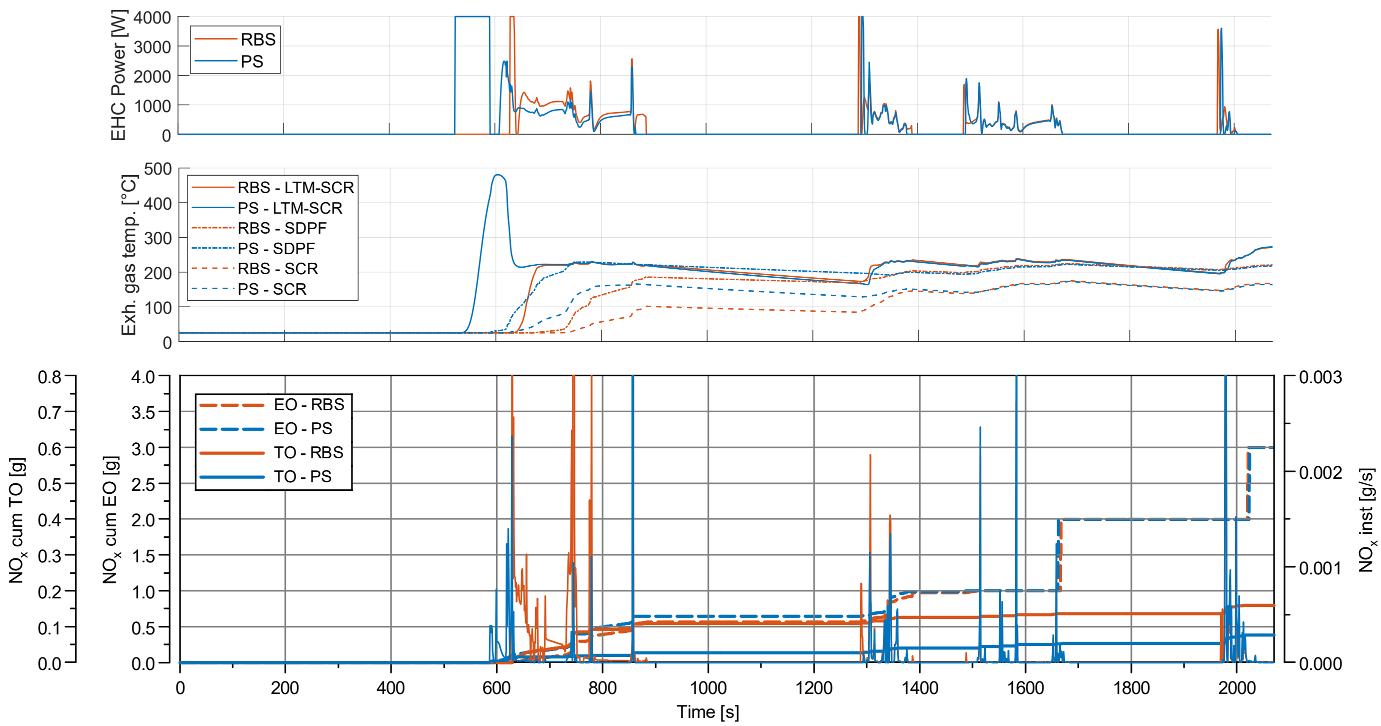

Figure 15 - Case 1: comparison between exhaust temperatures at LTM-SCR, SDPF, and SCR outlet for rule-based (red) and predictive (blue) EHC control strategies and corresponding EHC adsorbed power; on the bottom, resulting tailpipe NOx emission for the two considered EHC control strategies.

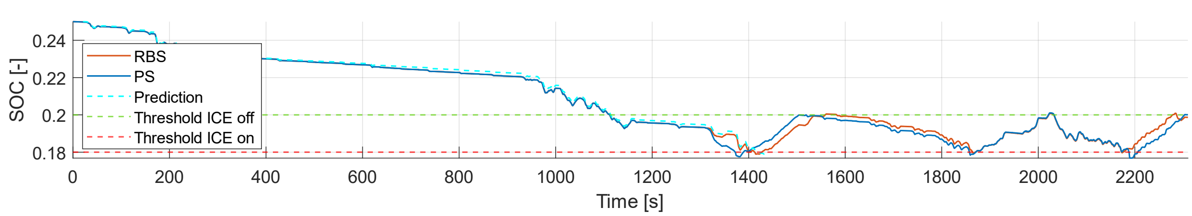

Figure 16 - Case 2: comparison of SoC traces for rule-based (red) and predictive (blue) EHC control strategies; cyan dashed line shows the SoC trace prediction. Lower and upper SoC thresholds below and above which ICE is turned on or off respectively are shown as well.

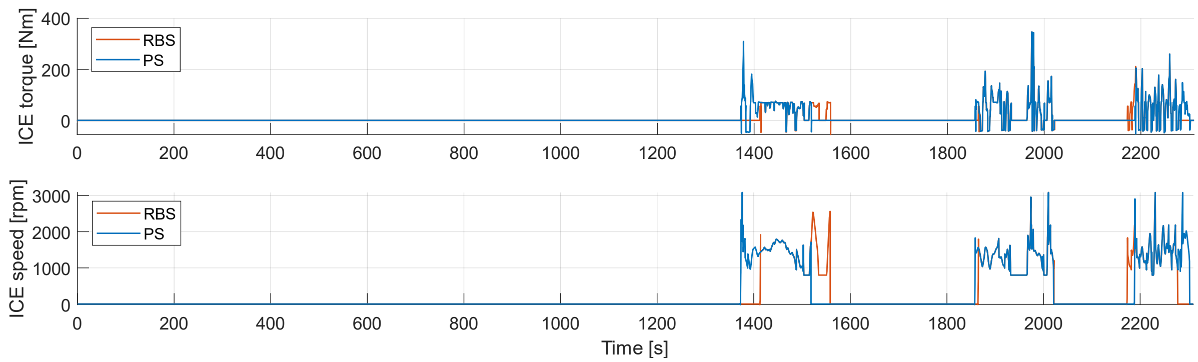

Figure 17 - Case 2: comparison of ICE speed and torque for rule-based (red) and predictive (blue) EHC control strategies.

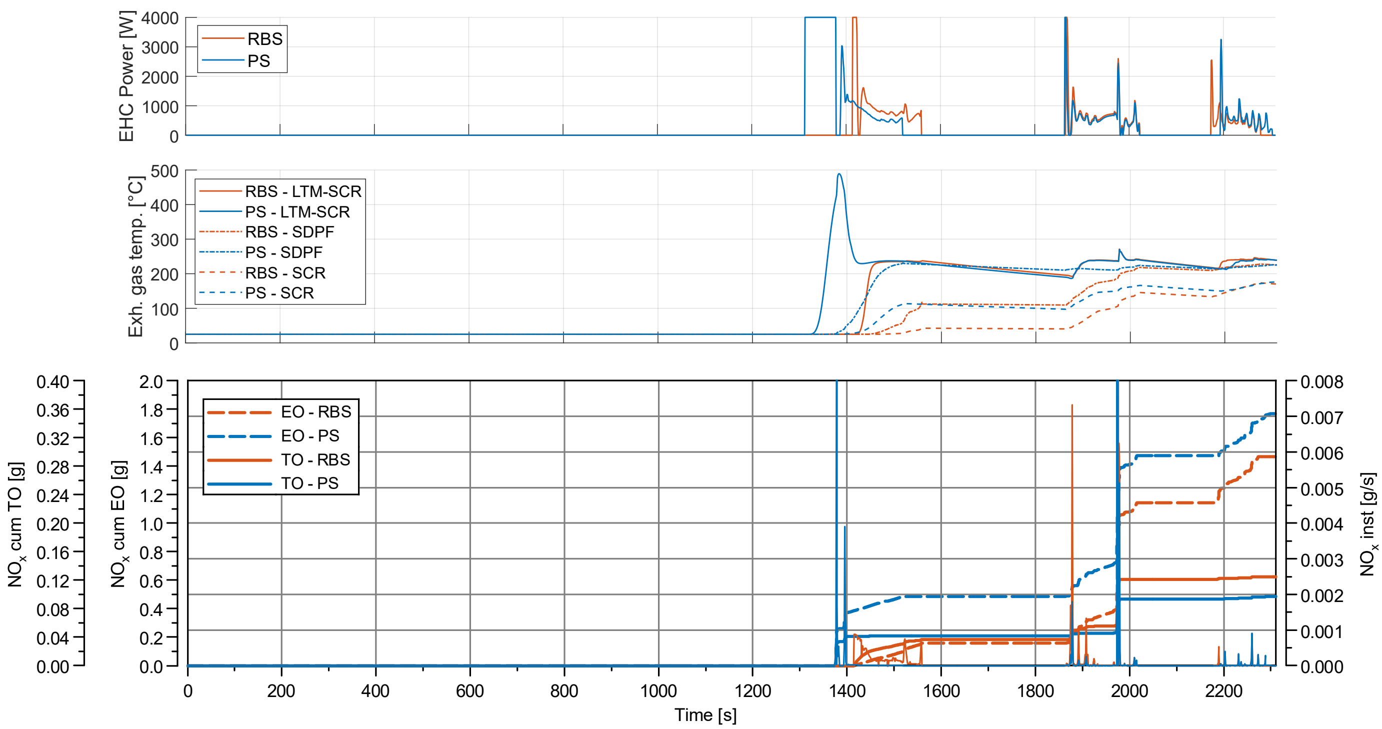

Figure 18 - Case 2: comparison of exhaust temperature at LTM-SCR, SDPF, and SCR outlet for rule-based (red) and predictive (blue) EHC control strategies and corresponding EHC adsorbed power; on the bottom, resulting tailpipe NOx emission for the two considered EHC control strategies.

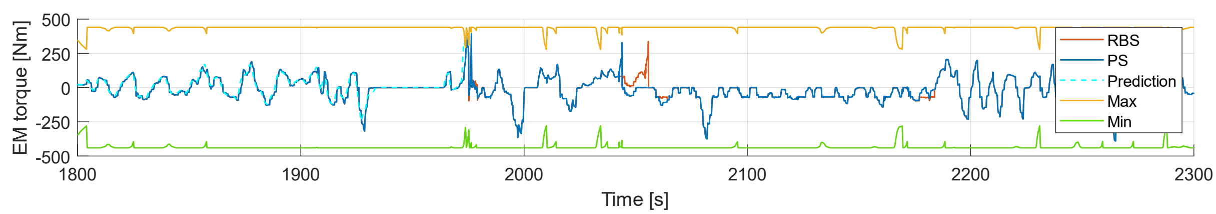

Figure 19 - Case 3: comparison of EM torque for rule-based (red) and predictive (blue) EHC control strategies in the last 500 seconds of the considered driving cycle; cyan dashed line shows EM torque prediction.

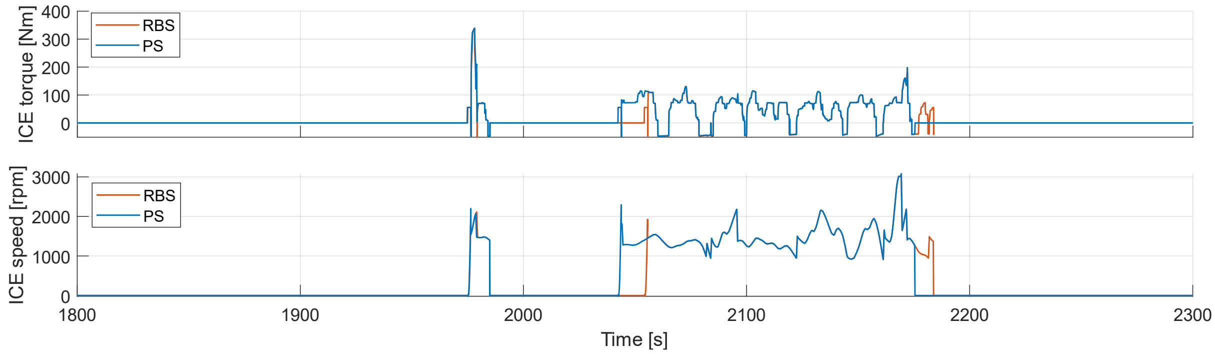

Figure 20 - Case 3: comparison of ICE speed and torque for rule-based (red) and predictive (blue) EHC control strategies in the last 500 seconds of the considered driving cycle.

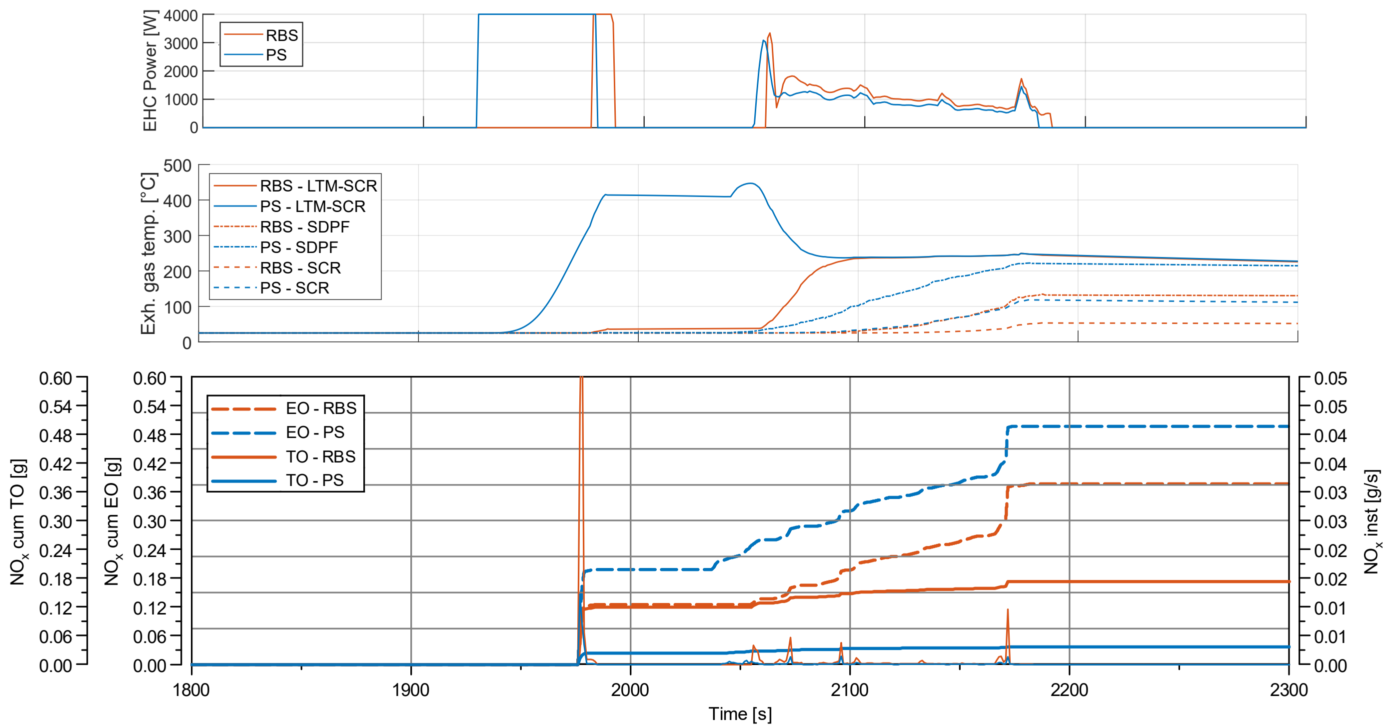

Figure 21 - Case 3: comparison of exhaust temperature at LTM-SCR, SDPF, and SCR outlet for rule-based (red) and predictive (blue) EHC control strategies and corresponding EHC adsorbed power in the last 500 seconds of the considered driving cycle; on the bottom, resulting tailpipe NOx emission for the two considered EHC control strategies.

3.4 Vehicle decontenting

Considering the less demanding Euro 7 scenario, referred to as "Scenario A" [31], the significant margin between the very low NO_x emissions obtained implementing an EHC predictive function and the limit imposed by the regulation (30 mg/km), paves the way to a simplification of the EATS layout to limit the related costs: part of the gain in terms of NO_x emission reduction can be converted into a cost saving resulting from a vehicle decontenting process. In this respect, the same rule-based and predictive control strategies have been applied to a simplified EATS layout without LTM-SCR. This layout modification is completely consistent with the implementation of an improved EATS thermal management strategy: the introduction of an electrical heater and especially of a pre-heating phase based on engine start prediction, allows to significantly speed up the heating of all EATS devices, thus making the installation of an additional SCR with reduced thermal inertia (LTM-SCR) less incisive from the point of view of limiting cold start tailpipe emissions. Moreover, the LTM-SCR removal results in a faster light-off of the SDPF and SCR catalyst, which will be installed closer to the DOC.

The results, represented in Figure 22, show that the average NO_x emissions, obtained performing the same simulations over RDE 1 and RDE 3 urban cycles, is still below the considered limit for all the test cases if the predictive EHC control strategy is applied. The removal of the LTM-SCR has a positive impact on the total cost of the EATS, which has been quantified by estimating the likely cost of each after-treatment device included in the exhaust line, according to the analysis carried out in [38]. As a final result, the implementation of the proposed predictive EHC control strategy allows to save approximately between the 12% and 13% of the EATS total manufacturing cost.

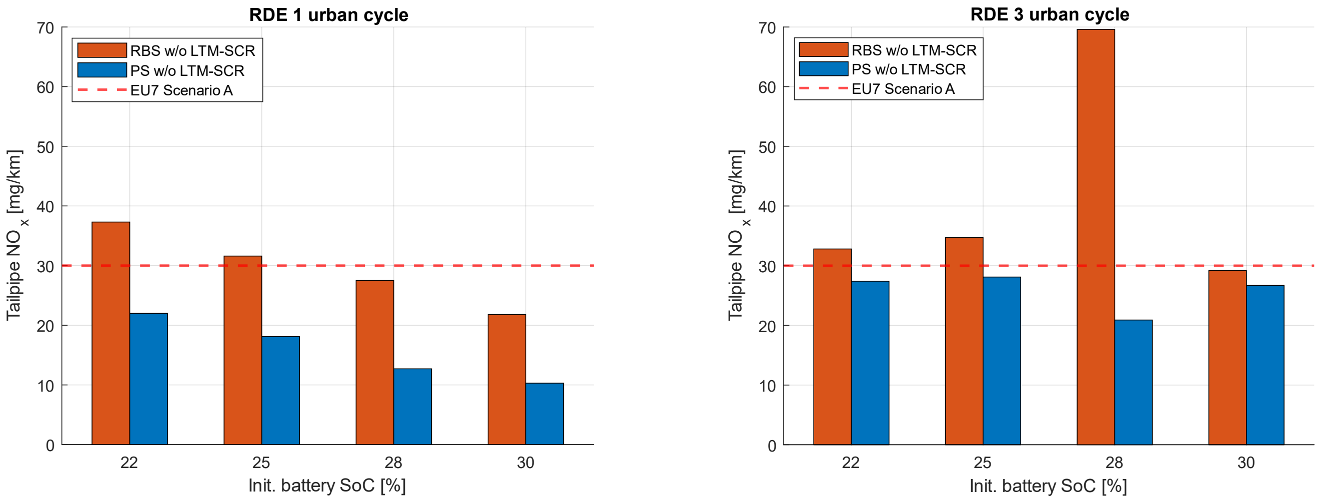

(**a**) (**b**)

Figure 22 – Average tailpipe NOx emission on RDE 1 cycle (a) and RDE 3 cycle (b) resulting from the rule-based strategy applied to the complete EATS layout, including LTM-SCR, and from the predictive strategy applied to a simplified EATS layout with no LTM-SCR.

4 Conclusions

The present activity has been focused on the development of a predictive EHC control function for a Diesel PHEV equipped with a state-of-the-art EATS. For this purpose, a comprehensive Simulink® model representative of the vehicle under study has been considered. As a first step, several simulations have been performed to evaluate the effect of EHC heating power and secondary air flow rate on the light-off time of the considered EATS components. Based on this analysis, the most convenient EATS heating strategy has been defined, aimed to minimize tailpipe NO_x emissions with limited additional energy consumption. In particular, a constant power of 4 kW has been provided to the EHC with constant secondary air flow rate of 55 kg/h for the whole duration of the pre-heating phase, which has been set to 60 seconds. A dedicated EHC control function has been implemented in the vehicle HCU to manage the planned EATS pre-heating phase based on ICE first start prediction. The proposed predictive control strategy has been tested on different urban driving scenarios, and the results discussed in section 0, highlight that:

- The introduction of a pre-heating phase allows to speed-up EATS warm up and improve NO_x conversion efficiency of LTM-SCR, SDPF, and SCR catalysts during engine cold start, always reducing the average NO_x emission over all the considered driving cycles with respect to the base EHC strategy, despite random events that may occur;

- The average NO_x emission achieved with the proposed predictive control strategy is reduced by more than 50% if compared to the base EHC strategy, except for few cases that have been commented in 3.2. Depending on the considered driving conditions, the NO_x emission reduction can reach values around the 70% for some of the considered cases;

- The EATS pre-heating phase requires additional energy to be provided to EHC, which is compensated by a greater use of the engine to recharge the battery, thus resulting in increased CO_2 emissions, which ranges from 1% to 10% with a single case that exceeds the 30%. This percentage increase is related to the specific driving conditions, since the impact of the pre-heating strongly depends on the total amount of emitted CO_2 and also on engine operating conditions along the considered cycle, that could be influenced by a different SoC trend and EATS temperature, as highlighted in section 0. Further research should be done to limit this significant cycle-dependence;

- Considering the foreseen future limits introduced by the Euro 7 proposal [31], the described EATS equipped with an EHC would be able to meet the NO_x emission target for LCVs even without the introduction of a predictive strategy if the less demanding “Scenario A” is considered, which will set the actual limit to 30 mg/km. Nevertheless, the improvement in NO_x emissions control enabled by the implementation of a predictive EHC control function would allow being compliant with the regulation in most of the considered cases even if this limit were lowered to 10 mg/km, according to the most stringent situation referred to as “Scenario B”;

- Thanks to the implementation of the proposed EHC predictive control strategy, the average tailpipe NO_x emissions can still be kept below the limit imposed by the less demanding Euro 7 scenario even considering a simplified EATS layout without LTM-SCR, thus allowing to reduce the corresponding EATS manufacturing cost.

Besides these promising results, which show the potential of including an EATS pre-heating based on ICE start prediction, the tests described in section 3 highlight that the final result may be strongly affected by the randomness of the occurring driving conditions. This issue must be solved in order to reach the robustness required in view of a real-world application of the proposed control strategy. Based on all these considerations, the developed predictive control strategy can be definitely considered a successful proof of concept to be used as a starting point for further improvements. In this respect, future research will be focused on developing a probabilistic approach that would evaluate ICE start probability within each road segment composing the complete driving cycle, rather than the exact time instant in which it should happen. This would help to solve the problem related to inevitable prediction inaccuracies and resulting random errors that may affect the final result, thus improving the robustness of the developed control strategy in view of HiL (Hardware-in-the-Loop) simulation and real-world application. In addition, further analysis could be performed by extending the temperature range of the considered test cases to evaluate the gain introduced by the predictive control strategy when very low ambient temperatures are considered. Finally, an important step would be to integrate the developed control function with additional predictive control strategies focused on energy management, in order to achieve the best results in terms of efficiency and pollutant emissions at the same time.

Nomenclature

Abbreviations

ADAS	Advanced Driver-Assistance Systems
BMEP	Brake Mean Effective Pressure
BSFC	Brake Specific Fuel Consumption
$BSNO_x$	Brake Specific NO_x
BVM	Backward Vehicle Model
CB	Charge Blended
CD	Charge-Depleting
CFD	Computational Fluid Dynamics
CS	Charge-Sustaining
DOC	Diesel Oxidizing Catalyst
DoE	Design of Experiments
EATS	Exhaust After-Treatment System
EHC	Electrically Heated Catalyst
EM	Electric Machine
EO	Engine-Out
HCU	Hybrid Control Unit
HEV	Hybrid Electric Vehicle
HiL	Hardware-in-the-Loop
HV	High Voltage
ICE	Internal Combustion Engine
ISC	In-Service Conformity
LCV	Light Commercial Vehicle
LPS	Load-Point Shift
PEMS	Portable Emissions Measurement System
PHEV	Plug-in Hybrid Electric Vehicle
PS	Predictive Strategy
RBS	Rule-Based Strategy
RDE	Real Driving Emissions
SCR	Selective Catalytic Reduction
SDPF	SCR-coated Diesel Particulate Filter
SoC	State of Charge
TP	Tailpipe-Out
V2X	Vehicle-to-Everything
WLTP	Worldwide Harmonized Light Vehicles Test Procedure

Roman Symbols

A_{ext}, A_{int}	External and internal brick surface
c_p	Specific heat capacity
h_{ext}, h_{int}	External and internal convective heat transfer coefficient
h_z	Specific enthalpy of the z chemical reaction
m_x	Mass of the *x* component
M_x	Molar mass of the *x* component
n_x	Moles of the *x* component
Nu, Nu_t	Nusselt number, corrected Nusselt number
$\dot{Q}$	Heat flow rate
Re	Reynolds number
T_{amb}, T_g, T_s	Ambient, gas, and solid temperature
$\bar{T}$	Average temperature

Greek symbols

β	NO_2/NO_x mass ratio
ϵ	Emissivity
ϵ_s	Gas heat transfer effectiveness in space
ϵ_t	Solid heat transfer effectiveness in time
λ_g	Gas thermal conductivity
σ	Stefan-Boltzmann constant

References

[1] Regulation (EU) 2019/631 of the European Parliament and of the Council of 17 April 2019 setting CO2 emission performance standards for new passenger cars and for new light commercial vehicles, and repealing Regulations (EC) No 443/2009 and (EU) No 510/2011 (Text with EEA relevance.), vol. 111. 2019. Accessed: Dec. 16, 2021. [Online]. Available: http://data.europa.eu/eli/reg/2019/631/oj/eng

[2] Commission Regulation (EU) 2016/427 of 10 March 2016 amending Regulation (EC) No 692/2008 as regards emissions from light passenger and commercial vehicles (Euro 6) (Text with EEA relevance), vol. 082. 2016. Accessed: Dec. 16, 2021. [Online]. Available: http://data.europa.eu/eli/reg/2016/427/oj/eng

[3] A. Tansini, J. Pavlovic, and G. Fontaras, “Quantifying the real-world CO2 emissions and energy consumption of modern plug-in hybrid vehicles,” Journal of Cleaner Production, vol. 362, p. 132191, Aug. 2022, doi: 10.1016/j.jclepro.2022.132191.

[4] J. Benajes, A. García, J. Monsalve-Serrano, and S. Martínez-Boggio, “Emissions reduction from passenger cars with RCCI plug-in hybrid electric vehicle technology,” Applied Thermal Engineering, vol. 164, p. 114430, Jan. 2020, doi: 10.1016/j.applthermaleng.2019.114430.

[5] R. Vignesh and B. Ashok, “Critical interpretative review on current outlook and prospects of selective catalytic reduction system for De-NOx strategy in compression ignition engine,” Fuel, vol. 276, p. 117996, Sep. 2020, doi: 10.1016/j.fuel.2020.117996.

[6] S. Rood, S. Eslava, A. Manigrasso, and C. Bannister, “Recent advances in gasoline three-way catalyst formulation: A review,” Proceedings of the Institution of Mechanical Engineers, Part D: Journal of Automobile Engineering, vol. 234, no. 4, pp. 936–949, 2020, doi: 10.1177/0954407019859822.

[7] S. Bagheri, Y. Huang, P. D. Walker, J. L. Zhou, and N. C. Surawski, “Strategies for improving the emission performance of hybrid electric vehicles,” Science of The Total Environment, vol. 771, p. 144901, Jun. 2021, doi: 10.1016/j.scitotenv.2020.144901.

[8] D. Thomas, H. Li, K. Ropkins, X. Wang, and Y. Ge, “Investigating the engine behavior of a hybrid vehicle and its impact on regulated emissions during on-road testing,” SAE Technical Paper 2019-01-2199, Apr. 2019, doi: 10.4271/2019-01-2199.

[9] S. I. Ehrenberger, M. Konrad, and F. Philipps, “Pollutant emissions analysis of three plug-in hybrid electric vehicles using different modes of operation and driving conditions,” Atmospheric Environment, vol. 234, p. 117612, Aug. 2020, doi: 10.1016/j.atmosenv.2020.117612.

[10] J. J. Eckert, S. F. da Silva, M. A. de M. Lourenço, F. C. Corrêa, L. C. A. Silva, and F. G. Dedini, “Energy management and gear shifting control for a hybridized vehicle to minimize gas emissions, energy consumption and battery aging,” Energy Conversion and Management, vol. 240, p. 114222, Jul. 2021, doi: 10.1016/j.enconman.2021.114222.

[11] Y. Wang et al., “Real driving energy consumption and CO2 & pollutant emission characteristics of a parallel plug-in hybrid electric vehicle under different propulsion modes,” Energy, vol. 244, p. 123076, Apr. 2022, doi: 10.1016/j.energy.2021.123076.

[12] J. Gao, G. Tian, A. Sorniotti, A. E. Karci, and R. Di Palo, “Review of thermal management of catalytic converters to decrease engine emissions during cold start and warm up,” Applied Thermal Engineering, vol. 147, pp. 177–187, Jan. 2019, doi: 10.1016/j.applthermaleng.2018.10.037.

[13] Y. Zeng, Y. Cai, C. Chu, G. Kou, and W. Gao, “Integrated Energy and Catalyst Thermal Management for Plug-In Hybrid Electric Vehicles,” Energies, vol. 11, no. 7, Art. no. 7, Jul. 2018, doi: 10.3390/en11071761.

[14] A. Guille des Buttes, B. Jeanneret, A. Kéromnès, L. Le Moyne, and S. Pélissier, “Energy management strategy to reduce pollutant emissions during the catalyst light-off of parallel hybrid vehicles,” Applied Energy, vol. 266, p. 114866, May 2020, doi: 10.1016/j.apenergy.2020.114866.

[15] M. R. Hamedi, O. Doustdar, A. Tsolakis, and J. Hartland, “Thermal energy storage system for efficient diesel exhaust aftertreatment at low temperatures,” Applied Energy, vol. 235, pp. 874–887, Feb. 2019, doi: 10.1016/j.apenergy.2018.11.008.

[16] M. S. Reiter and K. M. Kockelman, “The problem of cold starts: A closer look at mobile source emissions levels,” Transportation Research Part D: Transport and Environment, vol. 43, pp. 123–132, 2016, doi: 10.1016/j.trd.2015.12.012.

[17] M. R. Hamedi, O. Doustdar, A. Tsolakis, and J. Hartland, “Energy-efficient heating strategies of diesel oxidation catalyst for low emissions vehicles,” Energy, vol. 230, p. 120819, Sep. 2021, doi: 10.1016/j.energy.2021.120819.

[18] J. Gao, G. Tian, and A. Sorniotti, “On the emission reduction through the application of an electrically heated catalyst to a diesel vehicle,” Energy Science & Engineering, vol. 7, no. 6, pp. 2383–2397, 2019, doi: 10.1002/ese3.416.

[19] J. Hofstetter, P. Boucharel, F. Atzler, and G. Wachtmeister, “Fuel Consumption and Emission Reduction for Hybrid Electric Vehicles with Electrically Heated Catalyst,” SAE Int. J. Adv. & Curr. Prac. in Mobility, vol. 3, no. 1, Art. no. 2020-37–0017, Jun. 2020, doi: 10.4271/2020-37-0017.

[20] A. García, J. Monsalve-Serrano, R. Lago Sari, and S. Martinez-Boggio, “Energy assessment of an electrically heated catalyst in a hybrid RCCI truck,” Energy, vol. 238, p. 121681, Jan. 2022, doi: 10.1016/j.energy.2021.121681.

[21] B. Bargman, S. Jang, J. Kramer, I. Soliman, and A. A. A. M. Sahul, “Effects of Electrically Preheating Catalysts on Reducing High-Power Cold-Start Emissions,” SAE International, Warrendale, PA, SAE Technical Paper 2021-01–0572, Apr. 2021. doi: 10.4271/2021-01-0572.

[22] F. Mianzarasvand, A. Shirneshan, and M. Afrand, “Effect of electrically heated catalytic converter on emission characteristic of a motorcycle engine in cold-start conditions: CFD simulation and kinetic study,” Applied Thermal Engineering, vol. 127, pp. 453–464, 2017, doi: 10.1016/j.applthermaleng.2017.07.180.

[23] V. Schallhart, H. Berthold, E. Klemm, and L. Moeltner, “Light-Off Support for Mobile DeNOx Systems,” Chemie Ingenieur Technik, vol. 93, no. 5, pp. 814–818, 2021, doi: 10.1002/cite.202000212.

[24] A. Capancioni, L. Brunelli, N. Cavina, and A. Perazzo, “Development of Adaptive-ECMS and predictive functions for Plug-in HEVs to Handle Zero-Emission Zones Using Navigation Data,” SAE Technical Paper 2021-24-0105, Sep. 2021, doi: 10.4271/2021-24-0105.

[25] G. Caramia, N. Cavina, M. Caggiano, S. Patassa, and D. Moro, “Battery state of charge management strategies for a real-time controller of a Plug-in Hybrid Electric Vehicle,” Energy Procedia, vol. 148, pp. 258–265, Aug. 2018, doi: 10.1016/j.egypro.2018.08.076.

[26] G. Caramia, N. Cavina, A. Capancioni, M. Caggiano, and S. Patassa, “Combined Optimization of Energy and Battery Thermal Management Control for a Plug-in HEV,” SAE

International, Warrendale, PA, SAE Technical Paper 2019-24–0249, Oct. 2019. doi: 10.4271/2019-24-0249.
[27] J. Zhao and J. Wang, “Integrated Model Predictive Control of Hybrid Electric Vehicles Coupled With Aftertreatment Systems,” IEEE Transactions on Vehicular Technology, vol. 65, no. 3, pp. 1199–1211, Mar. 2016, doi: 10.1109/TVT.2015.2405918.
[28] T. Nüesch, A. Cerofolini, G. Mancini, N. Cavina, C. Onder, and L. Guzzella, “Equivalent Consumption Minimization Strategy for the Control of Real Driving NOx Emissions of a Diesel Hybrid Electric Vehicle,” Energies, vol. 7, no. 5, Art. no. 5, May 2014, doi: 10.3390/en7053148.
[29] M. Hopka, D. Upadhyay, and M. Van Nieuwstadt, “Smart DPF Regenerations - A Case Study of a Connected Powertrain Function,” SAE Int. J. Advances & Curr. Prac. in Mobility 1(2):762-770, pp. 2019-01–0316, Apr. 2019, doi: 10.4271/2019-01-0316.
[30] G. Caramia, N. Cavina, D. Moro, S. Patassa, and L. Solieri, “Predictive NOx emission control of a diesel-HEV for CO2 and urea consumption reduction,” AIP Conference Proceedings, vol. 2191, no. 1, p. 020035, Dec. 2019, doi: 10.1063/1.5138768.
[31] Z. Samaras, S. Hausberger, and D. G. Mellios, “Preliminary findings on possible Euro 7 emission limits for LD and HD vehicles,” presented at the Online AGVES Meeting, Oct. 27, 2020. [Online]. Available: https://circabc.europa.eu/
[32] ACEA, “ACEA Proposal for Euro7,” Jun. 2021. Accessed: Feb. 28, 2022. [Online]. Available: https://www.acea.auto/files/ACEA_proposal_for_Euro7.pdf
[33] Commission Regulation (EU) 2018/1832 of 5 November 2018 amending Directive 2007/46/EC of the European Parliament and of the Council, Commission Regulation (EC) No 692/2008 and Commission Regulation (EU) 2017/1151 for the purpose of improving the emission type approval tests and procedures for light passenger and commercial vehicles, including those for in-service conformity and real-driving emissions and introducing devices for monitoring the consumption of fuel and electric energy (Text with EEA relevance.), vol. 301. 2018. Accessed: Dec. 16, 2021. [Online]. Available: http://data.europa.eu/eli/reg/2018/1832/oj/eng
[34] G. Di Pierro, “Development of an integrated experimental and numerical methodology for the performance analysis of multiple hybrid electric architectures over different driving cycles,” Doctoral Dissertation, Politecnico di Torino, Turin, Italy, 2020. [Online]. Available: https://iris.polito.it/handle/11583/2843980?mode=full.13517#.YsXJeHZBxaQ
[35] A. Lubeski, “Real-Time Catalytic Converter Temperature Estimator in the Powertrain Controller,” SAE International, Warrendale, PA, SAE Technical Paper 2000-01–0651, Mar. 2000. doi: 10.4271/2000-01-0651.
[36] S. Meisner and S. C. Sorenson, “Computer Simulation of Intake and Exhaust Manifold Flow and Heat Transfer,” Warrendale, PA, May 1986. doi: 10.4271/860242.
[37] P. J. Shayler, D. J. Hayden, and T. Ma, “Exhaust System Heat Transfer and Catalytic Converter Performance,” SAE International, Warrendale, PA, SAE Technical Paper 1999-01–0453, Mar. 1999. doi: 10.4271/1999-01-0453.
[38] T. Dallmann, “Costs of Emission Reduction Technologies for Diesel Engines Used in Non-Road Vehicles and Equipment,” p. 26, Jul. 2018, Accessed: Oct. 01, 2021. [Online]. Available: https://theicct.org/sites/default/files/publications/Non_Road_Emission_Control_20180711.pdf

Appendix A

Engine model: fuel consumption and NOx emissions maps

The fuel consumption and engine-out NO_x emission maps provided below refer to the cold operation of the engine. The same trend is observed for warm conditions, showing lower values of fuel consumption and higher values of NO_x emission with respect to cold conditions, according to the different engine operation during warm up phases.

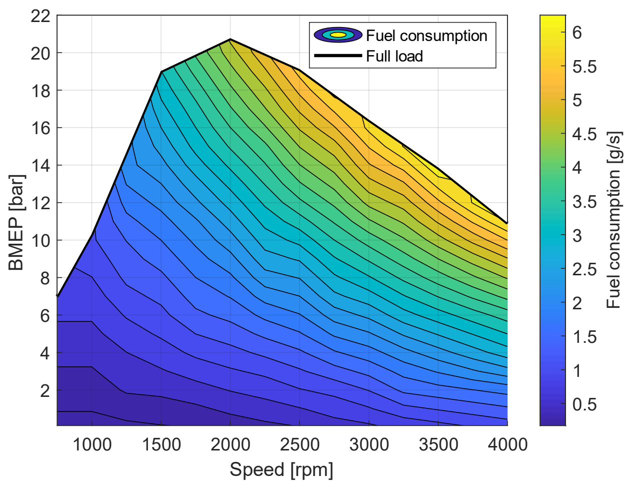

Figure A 1 – Fuel consumption map for engine cold operation as a function of engine speed and BMEP.

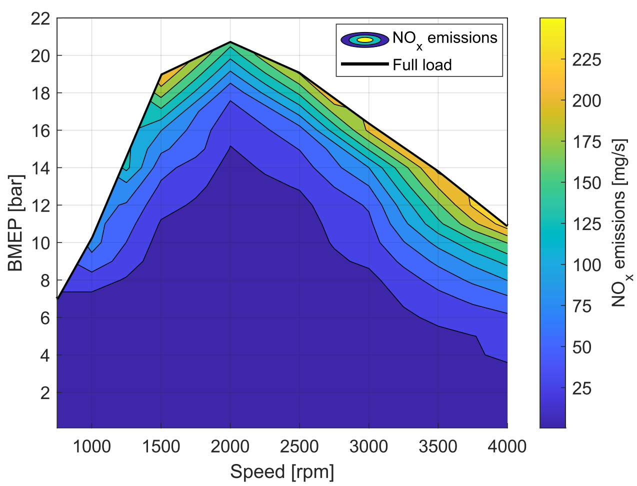

Figure A 2 – Engine-out NO_x emission map for engine cold operation as a function of engine speed and BMEP.

E-drive strategy: SoC thresholds definition

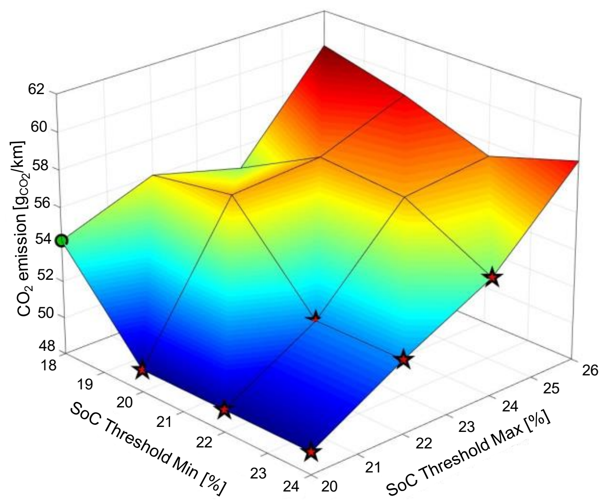

Figure A 3 - DoE analysis for SoC thresholds definition: resulting weighted CO_2 emission, selected configuration (green dot) and unviable configurations

Hybrid strategy: LPS maps

Three different LPS maps have been generated to manage the torque split between the ICE and the EM, following different targets depending on the operating conditions:

- Normal mode shift-down: this map provides the amount of torque requested to the EM (rather than to the ICE) in order to reach the BSFC target for each given engine speed. The aim is to reduce fuel consumption by using the EM to provide part of the driving torque, so that the engine works at lower load.
- Cat-heating mode shift-down: this map replaces the previous one during ICE and EATS warm-up phases, namely until the DOC temperature is above a minimum threshold, which is set to 180°C as for the e-drive condition. The amount of torque requested to the EM is calculated to reach the $BSNO_x$ target for each engine speed. The aim is to reduce NO_x engine-out emissions while the EATS is still cold and conversion efficiency is low.
- Normal / Cat-heating mode shift-up: this map provides the torque requested to the engine in addition to the driving torque, which is used to charge the battery. This torque value is calculated following an imposed exhaust gas temperature target, with the aim of having a fast EATS heating and to keep it warm after the heating phase. In this case the same load shift map is used for both normal and cat-heating mode.

Raw torque values derived from each map are then corrected by means of SoC-dependent factors which can vary in the range 0÷1, so that:

- ICE load shift-down is allowed only above a minimum SoC threshold, since the EM must be able to fulfill the driving torque that is not provided by the engine with no risk of damaging the battery reaching too low SoC;

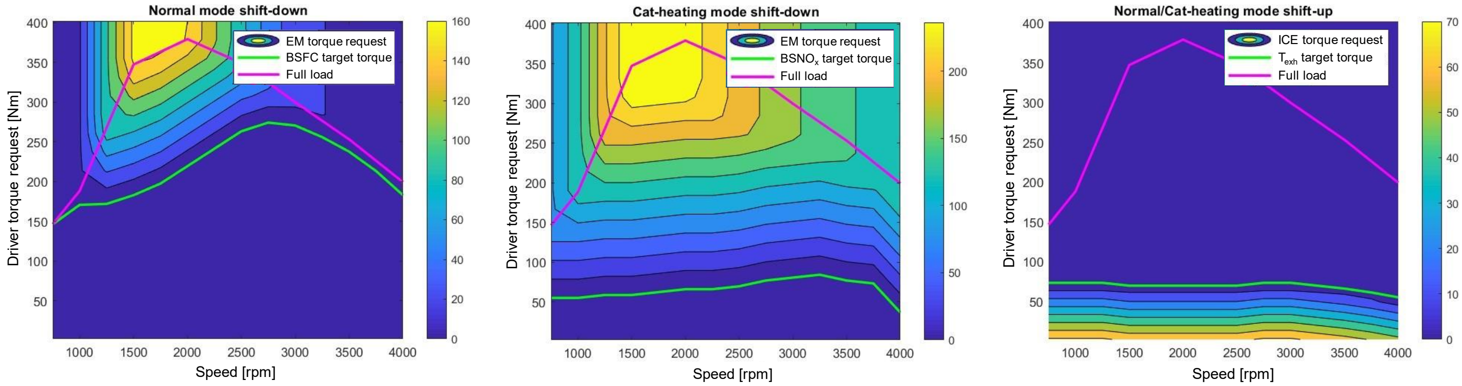

(**a**) (**b**) (**c**)

*Figure A 4 – LPS maps for torque split management in hybrid mode: normal mode shift-down map (**a**), cat-heating mode shift-down map (**b**), normal/cat-heating mode shift-up map (**c**).*

- ICE load shift-up is enabled only below a maximum SoC threshold, so that the additional torque provided by the engine can be used to charge the battery if it is not already charged.